Inference and reconstruction of the heimdallarchaeial ancestry of eukaryotes

Laura Eme[1,2▲], Daniel Tamarit[1,3,4▲†], Eva F. Caceres[1,3▲], Courtney W. Stairs[1††], Valerie De Anda[5], Max E. Schön[1], Kiley W. Seitz[5†††], Nina Dombrowski[5††††], William H. Lewis[1,3†††††], Felix Homa[3], Jimmy H. Saw[1††††††], Jonathan Lombard[1], Takuro Nunoura[6], Wen-Jun Li[7], Zheng-Shuang Hua[8], Lin-Xing Chen[9], Jillian F. Banfield[9,10], Emily St John[11], Anna-Louise Reysenbach[11], Matthew B. Stott[12], Andreas Schramm[13], Kasper U. Kjeldsen[13], Andreas P. Teske[14], Brett J. Baker[5,15], Thijs J. G. Ettema[1,3*]

[1]Department of Cell and Molecular Biology, Science for Life Laboratory, Uppsala University, 75123 Uppsala, Sweden

[2]Laboratoire Écologie, Systématique, Évolution, CNRS, Université Paris-Saclay, AgroParisTech, 91190 Gif-sur-Yvette, France

[3]Laboratory of Microbiology, Wageningen University and Research, 6708 WE Wageningen, The Netherlands

[4]Department of Aquatic Sciences and Assessment, Swedish University of Agricultural Sciences, SE-75007 Uppsala, Sweden

[5]Department of Marine Science, Marine Science Institute, University of Texas Austin, Port Aransas, TX, 78373, USA

[6]Research Center for Bioscience and Nanoscience (CeBN), Japan Agency for Marine-Earth Science and Technology (JAMSTEC), 2-15 Natsushima-cho, Yokosuka, 237-0061, Japan

[7]State Key Laboratory of Biocontrol, Guangdong Provincial Key Laboratory of Plant Resources and Southern Marine Science and Engineering Guangdong Laboratory (Zhuhai), School of Life Sciences, Sun Yat-Sen University, Guangzhou 510275, PR China

[8]Chinese Academy of Sciences Key Laboratory of Urban Pollutant Conversion, Department of Environmental Science and Engineering, University of Science and Technology of China, Hefei, 230026, PR China

[9]Department of Earth and Planetary Sciences, University of California, Berkeley, California, USA

[10]Department of Environmental Science, Policy, and Management, University of California, Berkeley, California, USA

[11]Department of Biology, Portland State University, Portland, Oregon, USA

[12]School of Biological Sciences, University of Canterbury, Christchurch, 8142, New Zealand

[13]Section for Microbiology, Department of Biology, Aarhus University, 8000 Aarhus, Denmark

[14]Department of Earth, Marine and Environmental Sciences, University of North Carolina, Chapel Hill, USA

[15]Department of Integrative Biology, University of Texas Austin, TX USA

*Correspondence to: thijs.ettema@wur.nl

▲Equal contribution

† Current address: Theoretical Biology and Bioinformatics, Department of Biology, Faculty of Science, Utrecht University, Padualaan 8, 3584CH Utrecht, The Netherlands

†† Current address: Department of Biology, Lund University, Sölvegatan 35, 223 62 Lund, Sweden

††† Current address: Structural and Computational Biology, European Molecular Biology Laboratory, Meyerhofstraße 1, 69117 Heidelberg, Germany

†††† Current address: NIOZ, Royal Netherlands Institute for Sea Research, Department of Marine Microbiology and Biogeochemistry; AB Den Burg, The Netherlands.

††††† Current address: Department of Biochemistry, University of Cambridge, Cambridge, CB2 1QW, UK

††††††: Current address: Department of Biological Sciences, The George Washington University, Washington, DC, USA

Abstract

In the ongoing debates about eukaryogenesis, the series of evolutionary events leading to the emergence of the eukaryotic cell from prokaryotic ancestors, members of the Asgard archaea play a key role as the closest archaeal relatives of eukaryotes. However, the nature and phylogenetic identity of the last common ancestor of Asgard archaea and eukaryotes remain unresolved. Here, we analyze distinct phylogenetic marker datasets of an expanded genomic sampling of Asgard archaea and evaluate competing evolutionary scenarios using state-of-the-art phylogenomic approaches. We find that eukaryotes are placed, with high confidence, as a well-nested clade within Asgard archaea, as a sister lineage to Hodarchaeales, a newly

proposed order within Heimdallarchaeia. Using sophisticated gene tree/species tree reconciliation approaches, we show that, in analogy to the evolution of eukaryotic genomes, genome evolution in Asgard archaea involved significantly more gene duplication and fewer gene loss events compared to other archaea. Finally, we infer that the last common ancestor of Asgard archaea likely was a thermophilic chemolithotroph, and that the lineage from which eukaryotes evolved adapted to mesophilic conditions and acquired the genetic potential to support a heterotrophic lifestyle. Our work provides key insights into the prokaryote-to-eukaryote transition and the platform for the emergence of cellular complexity in eukaryotic cells.

Main

Understanding how complex eukaryotic cells emerged from prokaryotic ancestors represents a major challenge in biology[1,2]. A main point of contention in refining eukaryogenesis scenarios revolves around the exact phylogenetic relationship between Archaea and eukaryotes. The use of phylogenomic approaches with improved models of sequence evolution combined with a much-improved archaeal taxon sampling – progressively unveiled by metagenomics – has recently yielded strong support for the "two-domain" tree of life, in which the eukaryotic clade branches from within Archaea[3–8]. The discovery of the first Lokiarchaeia genome provided additional evidence for the two-domain topology since this lineage was shown to represent, at the time, the closest relative of eukaryotes in phylogenomic analyses[9]. Moreover, Lokiarchaeia genomes were found to uniquely contain many genes encoding eukaryotic signature proteins (ESPs) –proteins involved in hallmark complex processes of the eukaryotic cell–, more so than any other prokaryotic lineage. The subsequent identification and analyses of several diverse relatives of Lokiarchaeia,

together forming the Asgard archaea superphylum, confirmed that Asgard archaea represented the closest archaeal relatives of eukaryotes[2,9,10]. Their exact evolutionary relationship to eukaryotes, however, remained unresolved: it has been unclear whether eukaryotes evolved from *within* Asgard archaea, or if they represented their sister-lineage[10]. Furthermore, two studies questioned this view of the tree of life altogether, suggesting that Asgard archaea represent a deep-branching Euryarchaeota-related clade[11,12], and that, in accordance with the "three-domain" tree, eukaryotes represent a sister group to all Archaea, although this was challenged[13,14]. A follow-up study that included an expanded taxonomic sampling of Asgard archaeal genome data failed to resolve the phylogenetic position of eukaryotes in the tree of life[15].

Here, we expand the genomic diversity of Asgard archaea by generating 63 novel Asgard metagenomic-assembled genomes (MAGs) from samples from 11 locations around the world. By analyzing the improved genomic sampling of Asgard archaea using state-of-the-art phylogenomics, including recently developed gene tree/species tree reconciliation approaches for ancestral genome content reconstruction, we firmly place eukaryotes nested within the Asgard archaea. By revealing key features regarding the identity, nature and physiology of the last Asgard archaea and eukaryotes common ancestor (LAECA), our results represent important, thus far missing pieces of the elusive eukaryogenesis puzzle.

Expanded Asgard archaea genomic diversity

To increase the genomic diversity of Asgard archaea, we sampled aquatic sediments and hydrothermal deposits from eleven geographically distinct sites (Supplementary Table 1, Supplementary Figure 1). After extraction and sequencing of total environmental DNA, we assembled and binned metagenomic reads into MAGs. Of these MAGs, 63 were found to belong

to the Asgard archaea superphylum, with estimated median completeness and redundancy of 83% and 4.2%, respectively (Supplementary Table 1). To assess the genomic diversity in this dataset, we reconstructed a phylogeny of ribosomal proteins encoded in a conserved 15-ribosomal protein (RP15) gene cluster[16] from these MAGs, and all publicly available Asgard archaea assemblies (retrieved June 29th, 2021; Figure 1). These analyses expand the genomic sampling across previously described major Asgard archaea clades (i.e., Loki-, Thor-, Heimdall-, Odin-, Hel-, Hermod-, Sif-, Jord- and Baldrarchaeia[9,10,15,17,18]) and recover a previously undescribed clade of high taxonomic rank (Candidatus Asgardarchaeia; see Ext. Data Fig. 1 and Supplementary Information for proposed uniformization of Asgard archaea taxonomic classification that will be adhered to throughout the present manuscript). We observed that the median estimated Asgard archaeal genome size (3.8 Mega basepairs (Mbp)) is considerably larger than those of representative genomes from TACK archaea and Euryarchaeota (median=1.8 Mbp for both) and DPANN archaea (median=1.2 Mbp) (Supplementary Table 1). Among Asgard archaea, Odinarchaeia display the smallest genomes (median=1.4 Mb), while Loki- and Helarchaeales contain the largest (median=4.3 Mbp for both). Unlike other major Asgard archaeal clades, Heimdallarchaeia possess a wide range of genome sizes, spanning from 1.6 to 7.4 Mbp (median=3.5 Mbp). Indeed, this large class contains five clades with diverse features. These include Njordarchaeales (median genome size=2.4 Mbp) followed by Kariarchaeaceae (median genome size=2.7 Mbp), Gerdarchaeales (median genome size=3.4 Mbp), Heimdallarchaeaceae (median genome size=3.7 Mbp), and finally Hodarchaeales (median genome size=5.1 Mbp). The smallest heimdallarchaeial genome corresponds to the only Asgard archaeal MAG recovered from a marine surface water metagenome (Heimdallarchaeota archaeon RS678)[19], in agreement with reduced genome sizes typically observed among prokaryotic plankton of the euphotic zone[20] .

Identification of phylogenetic conflict

Inferring deep evolutionary relationships in the tree of life is considered one of the hardest problems in phylogenetics. To interrogate the evolutionary relationships within the present set of Asgard archaeal phyla, and between Asgard archaea and eukaryotes, we performed an exhaustive range of sophisticated phylogenomic analyses. We analyzed a preexisting marker dataset comprising 56 concatenated ribosomal protein sequences (RP56)[9,10] for a phylogenetically diverse set of 331 archaeal (175 Asgard archaea, 41 DPANN, 43 Euryarchaeota, and 72 TACK archaea representatives), and 14 eukaryotic taxa (see Supplementary Table 2). Of note, the inclusion of an expanded diversity of 12 new Korarchaeota MAGs among these TACK archaea considerably affected phylogenomic analyses (see below). Initial maximum-likelihood (ML) phylogenetic inference based on this RP56 dataset confirmed the existence of 12 major Asgard archaeal clades of high taxonomic rank (Supplementary Figure 2). These include the previously described Loki-, Odin-, Heimdall-, Thor-[9,10], Helarchaeia[10], for which we here present 36 new genomes, and the recently proposed Sif-[18], Hermod-[17], Jord-[21], Wukong-[15] and Baldrarchaeia[15], for most of which we also identified new near-complete MAGs. Finally, we identified 15 MAGs representing the recently described Njordarchaeales[22] (which we show below is a divergent candidate order within Heimdallarchaeia), and a single MAG representing a new candidate class, Asgardarchaeia (which will be discussed in a separate manuscript; Tamarit et al, in prep) (Figure 1). Importantly, careful inspection of the obtained RP56 tree uncovered a potential artefact: Njordarchaeales, considered *bona fide* Asgard archaea based on the presence of many encoded 'typical' Asgard-like ESPs[10], were found to branch outside of the Asgard archaea, at the base of the TACK superphylum and as a sister lineage to Korarchaeota in the RP56 tree. In addition, eukaryotes were found to branch at

the base of the clade formed by Korarchaeota and Njordarchaeales, although with weak support. Hereafter, we focused on disentangling the historically correct phylogenetic signal from noise and artefacts.

Alternative phylogenomic markers

Despite often being used in phylogenomic analyses, ribosomal proteins have been suggested to contribute to phylogenetic artefacts due to inherent compositional sequence biases[23,24]. Additionally, considering the inconsistency of the obtained placement of eukaryotes compared to previous analyses, the incoherent placement of Njordarchaeales, and the presence of long branches at the base of both of these clades in the RP56 tree, we sought to use an alternative phylogenetic marker set to obtain a stable Asgard archaeal species tree, and to further investigate the phylogenetic position of eukaryotes. We constructed an independent 'new marker' dataset comprising 57 proteins of archaeal origin in eukaryotes (NM57 dataset; see Methods). The NM57 proteins are mostly involved in diverse informational, metabolic, and cellular processes, but do not include ribosomal proteins (Supplementary Table 2). Besides being longer, and hence putatively more phylogenetically informative compared to the RP56 markers, the broader functional distribution of NM57 markers is less likely to cause phylogenetic reconstruction artefacts induced by strong co-evolution between proteins – something that is to be expected for functionally and structurally cohesive ribosomal proteins[25]. Indeed, in case co-evolving protein sequences are compositionally biased, and hence violate evolutionary model assumptions of fixed composition over species, their concatenation is expected to strengthen the artefactual, non-phylogenetic signal and the statistical support for incorrect relationships[26]. We thus decided to independently evaluate the concatenated NM57 and RP56 marker datasets for downstream

phylogenomic analyses. We observed that ML phylogenomic analyses of the NM57 dataset did not only recover Njordarchaeales as *bona fide* Asgard archaea, they were also placed as the closest relatives of eukaryotes (BS=98%; Supplementary Figure 3), as was proposed in a recent analysis[22]. To investigate the underlying causes for the contradicting results between the NM57 and RP56 datasets, we first assessed the effect of taxon sampling on phylogenetic reconstructions by removing eukaryotic and/or DPANN and/or Korarchaeota sequences from the alignments, for two main reasons: (1) eukaryotes and DPANN archaea represent long-branching clades potentially inducing long branch attraction (LBA) artefacts; and (2) we wanted to investigate the effects of removing eukaryotes and Korarchaeota, which were the sister lineages of Njordarchaeales in the NM57 and RP56 phylogenetic analyses, respectively. Following this, we recoded the alignments into 4 states (using SR4-recoding[27]) to ameliorate potential phylogenetic artefacts arising from model misspecification at mutationally saturated or compositionally biased sites[14,28–30]. Further, with a similar goal, we applied a fast-evolving site removal (FSR) procedure to the concatenated datasets, since fast-evolving sites are often mutationally saturated. We performed phylogenetic analyses of the above-mentioned datasets in both ML and Bayesian Inference (BI) frameworks, under sophisticated evolutionary models that account for sequence heterogeneity in the substitution process across sites (mixture models; Supplementary Table 2).

Phylogenomic analyses of the above-mentioned combinations of taxon sampling, data treatments and phylogenetic frameworks revealed that Njordarchaeales are artefactually attracted to Korarchaeota in RP56 datasets (Supplementary Information). This attraction is likely caused by the high compositional similarity of njord- and korarchaeal RP56 ribosomal protein sequences, which is probably linked to their shared hyperthermophilic lifestyle (Supplementary Figures 4-6). Analyses of RP56 datasets from which Korarchaeota were removed, recovered Njordarchaeales as

an order at the base of or within Heimdallarchaeia (Supplementary Figure 7), consistent with phylogenomic analyses of the NM57 dataset that included Korarchaeota (Supplementary Figure 3). Next, in our efforts to resolve the phylogenetic placement of eukaryotes, we initially performed phylogenomic analyses on variations of the RP56 and NM57 datasets (Supplementary Table 2 and Discussion). However, since compared to the RP56 dataset, the NM57 dataset is larger and less compositionally biased, and is thus expected to have retained a stronger and more congruent phylogenetic signal, we focused the rest of our study on this more reliable dataset.

Eukarya represent a well-nested clade within Heimdallarchaeia

Subsequent phylogenetic analyses of untreated NM57 datasets with various taxon sampling variations recovered eukaryotes as sister-clade to Njordarchaeales in ML analyses (e.g., Supplementary Figure 3, Supplementary Table 2 and Supplementary information). However, ML analyses of the SR4-recoded datasets retrieved a complex phylogenetic signal, as in some cases eukaryotes were placed at the base of all Heimdallarchaeia (including Njordarchaeales) and Wukongarchaeia. This strongly suggests that the previously observed phylogenetic affiliation between Njordarchaeales and eukaryotes could represent an artefact. Furthermore, when both SR4-recoding and FSR treatments were combined, eukaryotes were nested within Heimdallarchaeia, as sister-group to the order Hodarchaeales (Figure 2; Supplementary Figure 8), and this position was supported by ML analyses of NM57 datasets across all taxon selection variations (removing DPANN archaea, and/or Korarchaeota and/or Njordarchaeales). Congruently, the monophyly of eukaryotes and Hodarchaeales was systematically recovered by BI of recoded datasets (both with and without FSR; Figure 2, Supplementary Table 2). In addition, the position of Njordarchaeales shifted during these analyses, moving from a deep position at the base of Heimdallarchaeia and

Wukongarchaeia, to a more nested position forming a clade with Gerdarchaeales and Kari- and Heimdallarchaeaceae (Supplementary Discussion). This shift is observed in both the NM57 and the RP56 datasets analyses when SR4-recoding and FSR was combined (Supplementary Figures 9-10), supporting that Njordarchaeales represent a divergent order-level lineage of Heimdallarchaeia.

In summary, resolving the position of eukaryotes relative to Asgard archaea is anything but trivial (see Supplementary Discussion). In our efforts to extract the true phylogenetic signal, we provide confident support for eukaryotes forming a well-nested clade within the Asgard archaea phylum, consistent with the 2D tree of life scenario. More specifically, we observe that eukaryotes affiliate with the Heimdallarchaeia in analyses in which we systematically reduce phylogenetic artefacts, predominantly converging on a position of eukaryotes as sister to Hodarchaeales, which is also in line with the observed ESP content and genome evolution dynamics (see below).

Informational ESPs in Hodarchaeales

We found that most of the ESPs previously identified in a limited sampling of Asgard archaea[9,10] are widespread across all phyla included in the present study (Figure 3, Supplementary Table 3). Notably, we observed some exceptions in support of the phylogenetic affiliation between Hodarchaeales and eukaryotes, particularly among ESPs involved in information processing: (1) the ε DNA polymerase subunit is only found in Hodarchaeales; (2) ribosomal protein L28e (Rpl28e/Mak16) homologs are unique to Njord- and Hodarchaeales members; (3) many archaea that lack genes coding for the synthesis of diphthamide, a modified histidine residue which is uniquely present in archaeal and eukaryotic elongation factor 2 (EF-2), instead encode a second EF-2 paralog that misses key-residues required for diphthamide modification[31]. Interestingly, we

found that among all Asgard archaea, only MAGs of all sampled Hodarchaeales members encode *dph* genes in addition to a single gene encoding canonical EF-2, which branches at the base of their eukaryotic counterparts in phylogenetic analyses (Supplementary Figure 11; Supplementary Information); (4) While RPL22e and RNA polymerase subunit RPB8 are found in several Asgard archaeal phyla, the only Heimdallarchaeia genomes encoding these genes are members of the Hodarchaeales. Finally, (5) we identified N-terminal histone tails characteristic of eukaryotic histones in all three Hodarchaeales MAGs, as well as in three Njordarchaeales genomes (see Supplementary Information). Altogether, the identification of these key-informational ESPs, in agreement with phylogenomic analyses described above, supports that Hodarchaeales represent the closest archaeal relatives of eukaryotes.

Expanded eukaryotic-like protein translocation repertoire

In our search for putative new ESPs in the expanded Asgard archaeal genomic diversity, we uncovered several additional homologs of proteins associated with the eukaryotic translocon, a protein complex primarily responsible for the post-translational modification of proteins, and subsequent insertion into, or transport across the membrane of the endoplasmic reticulum (ER)[32]. The eukaryotic translocon is comprised of the core Sec61 protein-conducting channel, and several accessory components, including the oligosaccharyltransferase (OST) and translocon-associated protein (TRAP) complexes (Figure 3b), both of which are involved in the biogenesis of N-glycosylated proteins[33]. The eukaryotic TRAP complex is composed of two to four subunits in eukaryotes. Using distant-homology detection methods, we identified homologs from three of these subunits to be broadly distributed across Asgard archaeal genomes, while the fourth one was detected only in a few thorarchaeial MAGs (Figure 3b). The eukaryotic OST complex generally

comprises 6-8 subunits organized into three subcomplexes that are collectively embedded in the ER membrane[34] (Figure 3b). Apart from STT3/AglB (OST subcomplex-II), which represents the catalytic subunit and is universally found across all three domains of life, other OST subcomplexes generally do not possess prokaryotic homologs beyond the Ost1/Ribophorin I (OST subcomplex-I) and Ost3/Tusc3 (OST subcomplex-II) subunits previously reported in Asgard archaea[10]. Here, we report the identification of Asgard archaeal homologs of all five additional subunits, Ost2/Dad1, Ost4, Ost5/TMEM258, SWP1/Ribophorin II and WBP1/Ost48. While we identified homologs of Ost4 and Ost5 (OST subcomplex-I) in most Asgard archaeal classes, the distribution of Ost2, WBP1, and Swp1, the first subcomplex-III subunits described in prokaryotes to date, was restricted to Heimdallarchaeia, including Njordarchaeales for WBP1, further supporting their monophyly. Our findings indicate that Asgard archaea and, by inference, LAECA, potentially encode relatively complex machineries for the N-linked glycosylation and translocation of proteins (Figure 3b).

Vesicular biogenesis and trafficking proteins

Intracellular vesicular transport represents a key process that emerged during eukaryogenesis. Previous studies have reported that Asgard archaeal genomes encode homologs of eukaryotic proteins comprising various intracellular vesicular trafficking and secretion machineries, including the ESCRT (endosomal sorting complexes required for transport), TRAPP (transport protein particle) and COPII (coat protein complex II) vesicle coatomer protein complexes[9,10]. Furthermore, as much as 2% of the genes of Asgard archaeal genomes were found to encode small GTPase homologs – a broad family of eukaryotic proteins, encompassing the Ras, Rab, Arf, Rho and Ran subfamilies, that are broadly implicated in budding, transport, docking and fusion of vesicles in

eukaryotic cells[9,10]. Here, we report the identification of Asgard archaeal homologs of subunits of additional vesicular trafficking complexes (Figure 3, Ext. Data Fig. 2, Supplementary Table 3). Noticeably, we found putative homologs of all four subunits composing eukaryotic adaptor proteins (AP) and coatomer protein (COPI) complexes, which, in eukaryotic cells, are involved in the formation of clathrin-coated pits and vesicles responsible for packaging and sorting cargo for transport through the secretory and endocytic pathways[35]. Those complexes are composed of two large subunits, belonging to the β- and γ-families, a medium μ-subunit, and a small σ-subunit. We found homologs of all functional domains composing those subunits, albeit sparsely distributed (Ext. Data Fig. 2, Supplementary Information). Additionally, we found homologs of several protein complexes involved in eukaryotic endosomal sorting such as the retromer, the HOPS/CORVET and the GARP complexes (Figure 3, red shading). Retromer is a coat-like complex associated with endosome-to-Golgi retrograde traffic[36] and we detected four of its five subunits in Asgard MAGs. One of these subunits is Vps5-BAR, which in Thorarchaeia is often fused to Vps28, a subunit of the ESCRT-I subcomplex, suggesting a functional link between BAR domain proteins and the thorarchaeial ESCRT complex. The GARP (Golgi-associated retrograde protein) complex is a multisubunit tethering complex located at the trans-Golgi network in eukaryotic cells, where it also functions to tether retrograde transport vesicles derived from endosomes[37,38], similarly to the retromer. GARP comprises four subunits, three of which we could detect in Asgard archaeal genomes, with a sparse and punctuated distribution. Functioning in opposite direction from the retromer and GARP complexes are the CORVET (Class C core vacuole/endosome tethering) and HOPS (Homotypic fusion and protein sorting) complexes[39]. Endosomal fusion and autophagy in eukaryotic cells depend on them and they share four core

262 subunits[40], three of which can be found in Asgard archaea, in addition to one of the HOPS specific
263 subunits[41].

264 Finally, while numerous components of the ESCRT-I, II and III systems have been previously
265 detected in Asgard archaea[9,10,42], we report here the identification of Asgard homologs for the
266 ESCRT-III regulators Vfa1, Vta1, Ist1, and Bro1.

267

268 **Ancestral Asgard archaea genome reconstruction**

269 The analysis of Asgard archaeal genome data obtained through metagenomics, combined with the
270 insights derived from cytological observations of the first two cultured Asgard archaea
271 '*Candidatus* Prometheoarchaeum syntrophicum'[43] and '*Candidatus* Lokiarchaeum ossiferum'[44],
272 have generated new hypotheses about the nature of the archaeal ancestor of eukaryotes[43,45–48].
273 However, these theories are mostly based on a limited number of features displayed by a single,
274 or a few Asgard archaeal lineages. While informative, features of present-day Asgard archaea do
275 not necessarily resemble those of LAECA, as these are potentially separated by over 2 Gya of
276 evolution[49]. Furthermore, Asgard archaeal phyla display a highly variable genome content with
277 respect to ESPs and predicted metabolic features[43,46,48,50,51], suggesting a complex evolutionary
278 history of those traits. In light of these considerations, we inferred ancestral features of LAECA
279 by using an ML evolutionary framework. We employed a recently developed probabilistic gene-
280 tree species-tree reconciliation approach[52,53] in combination with the extended taxonomic
281 sampling of Asgard archaeal genomes to reconstruct the evolutionary history of homologous gene
282 families and ancestral gene content across the Asgard archaeal species tree. For this, we inferred
283 ML phylogenetic trees of all 17,200 protein families encoded across 181 archaeal genomes,
284 including representatives from Asgard and TACK archaea, and Euryarchaeota clades. Importantly,

as missing genes and potential contaminations in MAGs will be regarded as recent gene loss and gain events in our ancestral reconstruction analyses, the use of incomplete MAGs with low contamination levels is unlikely to have a major impact on the inferred gene content of the deep archaeal ancestors that were reconstructed in the present study (also see Supplementary Information).

We first compared the distributions of estimated ancestral proteome sizes, and numbers of inferred gene duplications, losses and gains (i.e., horizontal gene transfers and originations) in all archaeal ancestral nodes (Supplementary Figure 12). Intriguingly, we observed that Heimdall- (and particularly the ancestor of Hodarchaeales) and Lokiarchaeia ancestors display significantly higher gene duplication rates compared to TACK and Euryarchaeota ancestors (Figure 4a). In addition, we found that most Asgard archaeal ancestors displayed gene loss rates comparable to other archaea, with the exception of Thorarchaeia, Lokiarchaeales and Jordarchaeia, which showed significantly lower loss rates. In agreement with the observed evolutionary genome dynamics, we found that predicted proteome sizes of most Asgard archaea ancestors are significantly larger than other archaeal ancestors ($P<0.001$), with Lokiarchaeia ancestors displaying the largest estimated proteome size (Supplementary Figure 13). Similarly, the Hodarchaeales ancestor had an estimated proteome size of 4,053 proteins, versus 3,134 for the last Asgard archaea common ancestor (LAsCA), reflecting the high duplication and low loss rates in that clade. The streamlined genome content of the Odinarchaeia ancestor represents an exception to the general trend of genome expansion across Asgard archaea, and possibly reflects an adaptation to high temperatures[54].

Ancestral features of LAECA

Using the approach described above, we also reconstructed the ancestral metabolic and physiological properties across the Asgard archaeal species tree, including the proposed closest archaeal relatives of eukaryotes, the Hodarchaeales. We infer that the LAsCA was a chemolithotroph that required the synthesis of organic building blocks via the Wood-Ljungdahl pathway (WLP) (Figure 4b and Supplementary information), for which we inferred the presence of key enzymes, including carbon monoxide dehydrogenase/acetyl-CoA synthase (CODH/ACS) and the formylmethanofuran dehydrogenase (FmdABCDE). In addition, our analyses revealed that the last common ancestors of individual Asgard archaeal phyla either had the genetic potential to switch between autotrophy and heterotrophy (Loki-, Thor-, Jord- and Baldrarchaeia) or a predominantly heterotrophic fermentative (Odin- and Heimdallarchaeia) lifestyle (Figure 4b, Supplementary Information). Specifically, we observed that the WLP was lost prior to the split between Njordarchaeales and the other Heimdallarchaeia (and therefore prior to the emergence of LAECA), indicating that LAECA was a heterotrophic fermenter (Supplementary Table 4).

Furthermore, we infer that the central carbon metabolism of Heimdallarchaeia (including Hodarchaeales) included the Embden-Meyerhof-Parnas (EMP) pathway and a partial oxidative pentose phosphate (OPP) pathway - both considered core modules of present-day eukaryotic central carbon metabolism. While the enzymes of these pathways in Asgard archaea do not share a common evolutionary origin with those of eukaryotes, this indicates that LAECA had a similar central carbon metabolism compared to modern eukaryotes (Supplementary Figure 14-15).

In addition, our analyses support the idea that the last common ancestor of Heimdallarchaeia contained several components of the electron transport chain (ETC)[48]. We inferred that the last common ancestor of Hodarchaeales likely contained CI, CII, CIV and a nitrate reductase complex

(NarGHIJ), indicating that nitrate might have been used as a terminal electron acceptor to perform anaerobic respiration. As such, the last Hodarchaeales common ancestor likely generated ATP using an electron transport chain where electrons from NADH and succinate were transferred through a series of membrane-associated complexes with quinones and cupredoxins as electron carriers to ultimately reduce nitrate[55].

As indicated above, a significant fraction of the currently sampled Asgard archaea diversity originates from geothermal or hydrothermal environments. Indeed, using an algorithm based on genome-derived features[56], we confirmed that (most) Njordarchaeales, Baldr- and Jordarchaeia are hyperthermophiles, Odinarchaeia are thermophiles, and Loki- and Thorarchaeia are mesophiles (Figure 4c, Supplementary Table 5). While Heimdallarchaeia seem to contain both meso- and thermophiles, we infer a mesophilic physiology for Hodarchaeales, obtaining the lowest predicted optimal growth temperatures among all Asgard archaea (median=36.7 °C). Asgard archaeal hyperthermophiles contain reverse gyrase, a topoisomerase that is typically encoded by hyperthermophilic prokaryotes[57]. We infer that a reverse gyrase was possibly present in LAsCA and that it was subsequently lost in all heimdallarchaeial orders except for Njordarchaeales. This observation would be compatible with a scenario in which Asgard archaea have a hyperthermophilic ancestry, but in which eukaryotes evolved from an Asgard archaea lineage that had adapted to mesophilic growth temperatures.

Discussion

Beyond genomic exploration, several studies have started to unveil important physiological, cytological and ecological aspects of Asgard archaea[43,58–60]. Yet, while such insights are certainly relevant, the cellular and physiological characteristics of present-day Asgard archaea will almost

certainly not resemble those of LAECA. Therefore, inferences about the identity and nature of LAECA and the process of eukaryogenesis should be made within an evolutionary context. We used an evolutionary framework to analyze an expanded Asgard archaeal genomic diversity, comprising 11 clades of high taxonomic rank. Using comprehensive phylogenomic analyses involving the evaluation of distinct marker protein datasets and systematic assessment of suspected phylogenetic artefacts and state-of-the-art models of evolution, we identified Hodarchaeales, a class-level clade within the Heimdallarchaeia, as the closest relatives of eukaryotes. Evidently, phylogenomic analyses aiming to pinpoint the phylogenetic position of eukaryotes in the tree of life are extremely challenging, and our results stress the importance of testing for possible sources of bias affecting phylogenomic reconstructions, as was recently reviewed[61]. The implementation of a probabilistic gene tree/species tree reconciliation approach allowed us to infer the evolutionary dynamics and ancestral content across the archaeal species tree providing several new insights into the Asgard archaeal roots of eukaryotes. Altogether, our results reveal a picture in which the Asgard archaeal ancestor of eukaryotes had, compared to other archaea, a relatively large genome, resulting mainly from more numerous gene duplication and fewer gene loss events. It is tempting to speculate that the elevated gene duplication rates observed in our analyses represent an ancestral feature of LAECA, and that it remained the predominant modus of genome evolution during the early stages of eukaryogenesis. We also inferred that the duplicated gene content of LAECA included several protein families involved in cytoskeletal and membrane-trafficking functions, including among others actin homologs, ESCRT complex subunits and small GTPase homologs. Our findings complement those of another study[62] reporting that eukaryotic proteins with an Asgard archaeal provenance, as opposed to those inherited from the mitochondrial symbiont,

374 duplicated the most during eukaryogenesis, particularly proteins of cytoskeletal and membrane-
375 trafficking families.

376 Beyond genome dynamics, our analyses of inferred ancestral genome content across the Asgard
377 archaeal species tree indicates that, while Asgard archaea likely had a thermophilic ancestry, the
378 lineage from which eukaryotes evolved was adapted to mesophilic conditions, which is compatible
379 with a generally assumed mesophilic ancestry of eukaryotes. Furthermore, we infer that LAECA
380 had the genetic potential to support a heterotrophic lifestyle, and may have been able to conserve
381 energy via nitrate respiration. In addition, based on taxonomic distribution and evolutionary
382 history of ESPs we show that complex pathways involved in protein targeting and membrane
383 trafficking, and in genome maintenance and expression in eukaryotes were inherited from their
384 Asgard archaeal ancestor. Of note, we identified additional Asgard archaeal homologs of
385 eukaryotic vesicular trafficking complex components. Of these, some Asgard archaeal proteins
386 display sequence similarity to proteins which, in eukaryotes, are part of the clathrin adaptor protein
387 complexes and of the COPI complex. These complexes are particularly interesting since they are
388 involved in the biogenesis of vesicles responsible for sorting cargo and subsequent transport
389 through the secretory and endocytic pathways[35]. Altogether, these results further suggest a
390 potential for membrane deformation, and possibly trafficking, in Asgard archaea. The ability to
391 deform membranes was recently shown in two papers reporting the first cultivated Lokiarchaeia
392 lineages, '*Ca.* P. syntrophicum strain MK-D1'[43] and '*Ca.* Lokiarchaeum ossiferum'[44], whose cells
393 both displayed unique morphological complexity including long and often branching protrusions
394 facilitated by a dynamic actin cytoskeleton. Thus far no[43], or only limited[44] visible endomembrane
395 structures were observed in these first cultured representatives of Asgard archaea. However, it is
396 important to restate here that, being separated by some 2 Gya of evolution, the cellular features of

present-day Asgard archaeal lineages do not necessarily resemble those of LAECA. Furthermore, given the disparity of the distribution patterns of membrane trafficking homologs in Asgard archaea, it will be crucial to isolate representatives of phyla other than Lokiarchaeia and study their cell biological features and potential for endomembrane biogenesis. Of particular interest would be members of the Heimdallarchaeia, and specifically Hodarchaeales, as the currently identified closest relatives of eukaryotes, as well as Thorarchaeia lineages, which seem to generally contain a particularly rich suite of homologs of eukaryotic membrane trafficking proteins.

By phylogenetically placing eukaryotes as a firmly-nested clade within the presently identified Asgard archaeal diversity, and by inferring ancestral genomic content across the Asgard archaea, our work provides insights into the identity and nature of the Asgard archaeal ancestor of eukaryotes, guiding future studies aiming to uncover new pieces of the elusive eukaryogenesis puzzle.

References

1. López-García, P. & Moreira, D. Open Questions on the Origin of Eukaryotes. *Trends Ecol. Evol.* **30**, 697–708 (2015).
2. Eme, L., Spang, A., Lombard, J., Stairs, C. W. C. W. & Ettema, T. J. G. T. J. G. Archaea and the origin of eukaryotes. *Nat. Rev. Microbiol.* **15**, nrmicro–2017 (2017).
3. Guy, L. & Ettema, T. J. G. The archaeal 'TACK' superphylum and the origin of eukaryotes. *Trends Microbiol.* **19**, 580–587 (2011).
4. Kelly, S., Wickstead, B. & Gull, K. Archaeal phylogenomics provides evidence in support of a methanogenic origin of the Archaea and a thaumarchaeal origin for the eukaryotes. *Proc. Biol. Sci.* **278**, 1009–1018 (2011).

5. Williams, T. a., Foster, P. G., Cox, C. J. & Embley, T. M. An archaeal origin of eukaryotes supports only two primary domains of life. *Nature* **504**, 231–236 (2013).

6. Lasek-Nesselquist, E. & Gogarten, J. P. The effects of model choice and mitigating bias on the ribosomal tree of life. *Mol. Phylogenet. Evol.* (2013) doi:10.1016/j.ympev.2013.05.006.

7. Raymann, K., Brochier-Armanet, C. & Gribaldo, S. The two-domain tree of life is linked to a new root for the Archaea. *Proceedings of the National Academy of Sciences* 201420858 (2015).

8. Cox, C. J., Foster, P. G., Hirt, R. P., Harris, S. R. & Embley, T. M. The archaebacterial origin of eukaryotes. *Proc. Natl. Acad. Sci. U. S. A.* **105**, 20356–20361 (2008).

9. Spang, A. *et al.* Complex archaea that bridge the gap between prokaryotes and eukaryotes. *Nature* **521**, 173–179 (2015).

10. Zaremba-Niedzwiedzka, K. *et al.* Asgard archaea illuminate the origin of eukaryotic cellular complexity. *Nature* **541**, 353–358 (2017).

11. Cunha, V. D. *et al.* Lokiarchaea are close relatives of Euryarchaeota, not bridging the gap between prokaryotes and eukaryotes. *PLOS Genetics* vol. 13 e1006810 Preprint at https://doi.org/10.1371/journal.pgen.1006810 (2017).

12. Da Cunha, V., Gaia, M., Nasir, A. & Forterre, P. Asgard archaea do not close the debate about the universal tree of life topology. *PLoS genetics* vol. 14 e1007215 (2018).

13. Spang, A. *et al.* Asgard archaea are the closest prokaryotic relatives of eukaryotes. *PLoS Genet.* **14**, (2018).

14. Williams, T. A., Cox, C. J., Foster, P. G., Szöllősi, G. J. & Embley, T. M. Phylogenomics provides robust support for a two-domains tree of life. *Nat Ecol Evol* **4**, 138–147 (2020).

15. Liu, Y. *et al.* Expanded diversity of Asgard archaea and their relationships with eukaryotes. *Nature* **593**, 553–557 (2021).

16. Hug, L. A. *et al.* Community genomic analyses constrain the distribution of metabolic traits across the Chloroflexi phylum and indicate roles in sediment carbon cycling. *Microbiome* **1**, 22 (2013).

17. Zhang, J.-W. *et al.* Newly discovered Asgard archaea Hermodarchaeota potentially degrade alkanes

and aromatics via alkyl/benzyl-succinate synthase and benzoyl-CoA pathway. *ISME J.* (2021) doi:10.1038/s41396-020-00890-x.

18. Farag, I. F., Zhao, R. & Biddle, J. F. 'Sifarchaeota' a novel Asgard phylum from Costa Rica sediment capable of polysaccharide degradation and anaerobic methylotrophy. *Appl. Environ. Microbiol.* (2021).
19. Tully, B. J., Graham, E. D. & Heidelberg, J. F. The reconstruction of 2,631 draft metagenome-assembled genomes from the global oceans. *Sci Data* **5**, 170203 (2018).
20. Swan, B. K. *et al.* Prevalent genome streamlining and latitudinal divergence of planktonic bacteria in the surface ocean. *Proc. Natl. Acad. Sci. U. S. A.* **110**, 11463–11468 (2013).
21. Sun, J. *et al.* Recoding of stop codons expands the metabolic potential of two novel Asgardarchaeota lineages. *ISME Communications* **1**, 1–14 (2021).
22. Xie, R. *et al.* Expanding Asgard members in the domain of Archaea sheds new light on the origin of eukaryotes. *Sci. China Life Sci.* **65**, 818–829 (2022).
23. Ribosomal proteins: Toward a next generation standard for prokaryotic systematics? *Mol. Phylogenet. Evol.* **75**, 103–117 (2014).
24. Petitjean, C., Deschamps, P., López-García, P. & Moreira, D. Rooting the Domain Archaea by Phylogenomic Analysis Supports the Foundation of the New Kingdom Proteoarchaeota. *Genome Biol. Evol.* **7**, 191–204 (2014).
25. Anishchenko, I., Ovchinnikov, S., Kamisetty, H. & Baker, D. Origins of coevolution between residues distant in protein 3D structures. *Proc. Natl. Acad. Sci. U. S. A.* **114**, 9122–9127 (2017).
26. Foster, P. G. & Hickey, D. A. Compositional bias may affect both DNA-based and protein-based phylogenetic reconstructions. *J. Mol. Evol.* **48**, (1999).
27. Susko, E. & Roger, A. J. On reduced amino acid alphabets for phylogenetic inference. *Mol. Biol. Evol.* **24**, 2139–2150 (2007).
28. Brown, M. W. *et al.* Phylogenomics demonstrates that breviate flagellates are related to opisthokonts and apusomonads. *Proceedings of the Royal Society B: Biological Sciences* **280**, 20131755–

20131755 (2013).

29. Jeffroy, O., Brinkmann, H., Delsuc, F. & Philippe, H. Phylogenomics: the beginning of incongruence? *Trends in Genetics* vol. 22 225–231 Preprint at https://doi.org/10.1016/j.tig.2006.02.003 (2006).

30. Viklund, J., Ettema, T. J. G. & Andersson, S. G. E. Independent Genome Reduction and Phylogenetic Reclassification of the Oceanic SAR11 Clade. *Molecular Biology and Evolution* vol. 29 599–615 Preprint at https://doi.org/10.1093/molbev/msr203 (2012).

31. Narrowe, A. B. *et al.* Complex Evolutionary History of Translation Elongation Factor 2 and Diphthamide Biosynthesis in Archaea and Parabasalids. *Genome Biol. Evol.* **10**, 2380–2393 (2018).

32. Wang, L. & Dobberstein, B. Oligomeric complexes involved in translocation of proteins across the membrane of the endoplasmic reticulum. *FEBS Lett.* **457**, 316–322 (1999).

33. Pfeffer, S. *et al.* Dissecting the molecular organization of the translocon-associated protein complex. *Nat. Commun.* **8**, 14516 (2017).

34. Bai, L., Wang, T., Zhao, G., Kovach, A. & Li, H. The atomic structure of a eukaryotic oligosaccharyltransferase complex. *Nature* **555**, 328–333 (2018).

35. Rout, M. P. & Field, M. C. The Evolution of Organellar Coat Complexes and Organization of the Eukaryotic Cell. *Annu. Rev. Biochem.* **86**, 637–657 (2017).

36. Seaman, M. N. J. The retromer complex - endosomal protein recycling and beyond. *J. Cell Sci.* **125**, 4693–4702 (2012).

37. Liewen, H. *et al.* Characterization of the human GARP (Golgi associated retrograde protein) complex. *Exp. Cell Res.* **306**, 24–34 (2005).

38. Pérez-Victoria, F. J. *et al.* Structural basis for the wobbler mouse neurodegenerative disorder caused by mutation in the Vps54 subunit of the GARP complex. *Proc. Natl. Acad. Sci. U. S. A.* **107**, 12860–12865 (2010).

39. Villaseñor, R., Kalaidzidis, Y. & Zerial, M. Signal processing by the endosomal system. *Curr. Opin. Cell Biol.* **39**, 53–60 (2016).

40. Graham, S. C. *et al.* Structural basis of Vps33A recruitment to the human HOPS complex by Vps16. *Proc. Natl. Acad. Sci. U. S. A.* **110**, 13345–13350 (2013).

41. Jiang, P. *et al.* The HOPS complex mediates autophagosome–lysosome fusion through interaction with syntaxin 17. *Molecular Biology of the Cell* vol. 25 1327–1337 Preprint at https://doi.org/10.1091/mbc.e13-08-0447 (2014).

42. Hatano, T. *et al.* Asgard archaea shed light on the evolutionary origins of the eukaryotic ubiquitin-ESCRT machinery. *Nat. Commun.* **13**, 3398 (2022).

43. Imachi, H. *et al.* Isolation of an archaeon at the prokaryote-eukaryote interface. *Nature* **577**, 519–525 (2020).

44. Rodrigues-Oliveira, T. *et al.* Actin cytoskeleton and complex cell architecture in an Asgard archaeon. *Nature* Preprint at https://doi.org/10.1038/s41586-022-05550-y (2022).

45. Sousa, F. L., Neukirchen, S., Allen, J. F., Lane, N. & Martin, W. F. Lokiarchaeon is hydrogen dependent. *Nat Microbiol* **1**, 16034 (2016).

46. Bulzu, P.-A. *et al.* Casting light on Asgardarchaeota metabolism in a sunlit microoxic niche. *Nature Microbiology* vol. 4 1129–1137 Preprint at https://doi.org/10.1038/s41564-019-0404-y (2019).

47. López-García, P. & Moreira, D. The Syntrophy hypothesis for the origin of eukaryotes revisited. *Nat Microbiol* **5**, 655–667 (2020).

48. Spang, A. *et al.* Proposal of the reverse flow model for the origin of the eukaryotic cell based on comparative analyses of Asgard archaeal metabolism. *Nat Microbiol* **4**, 1138–1148 (2019).

49. Betts, H. C. *et al.* Integrated genomic and fossil evidence illuminates life's early evolution and eukaryote origin. *Nat Ecol Evol* **2**, 1556–1562 (2018).

50. Seitz, K. W. *et al.* Asgard archaea capable of anaerobic hydrocarbon cycling. *Nat. Commun.* **10**, 1822 (2019).

51. Liu, Y. *et al.* Comparative genomic inference suggests mixotrophic lifestyle for Thorarchaeota. *ISME J.* **12**, 1021–1031 (2018).

52. Szöllõsi, G. J., Rosikiewicz, W., Boussau, B., Tannier, E. & Daubin, V. Efficient exploration of the

space of reconciled gene trees. *Syst. Biol.* **62**, 901–912 (2013).

53. Szöllősi, G. J., Davín, A. A., Tannier, E., Daubin, V. & Boussau, B. Genome-scale phylogenetic analysis finds extensive gene transfer among fungi. *Philos. Trans. R. Soc. Lond. B Biol. Sci.* **370**, 20140335 (2015).

54. Sabath, N., Ferrada, E., Barve, A. & Wagner, A. Growth Temperature and Genome Size in Bacteria Are Negatively Correlated, Suggesting Genomic Streamlining During Thermal Adaptation. *Genome Biol. Evol.* **5**, 966–977 (2013).

55. Savelieff, M. G. *et al.* Experimental evidence for a link among cupredoxins: red, blue, and purple copper transformations in nitrous oxide reductase. *Proc. Natl. Acad. Sci. U. S. A.* **105**, 7919–7924 (2008).

56. Sauer, D. B. & Wang, D.-N. Predicting the optimal growth temperatures of prokaryotes using only genome derived features. *Bioinformatics* Preprint at https://doi.org/10.1093/bioinformatics/btz059 (2019).

57. Pavel Lulchev, D. K. Reverse gyrase—recent advances and current mechanistic understanding of positive DNA supercoiling. *Nucleic Acids Res.* **42**, 8200 (2014).

58. Akıl, C. & Robinson, R. C. Genomes of Asgard archaea encode profilins that regulate actin. *Nature* **562**, 439–443 (2018).

59. Orsi, W. D. *et al.* Metabolic activity analyses demonstrate that Lokiarchaeon exhibits homoacetogenesis in sulfidic marine sediments. *Nat Microbiol* **5**, 248–255 (2020).

60. Neveu, E., Khalifeh, D., Salamin, N. & Fasshauer, D. Prototypic SNARE Proteins Are Encoded in the Genomes of Heimdallarchaeota, Potentially Bridging the Gap between the Prokaryotes and Eukaryotes. *Curr. Biol.* **30**, 2468–2480.e5 (2020).

61. Williams, T. A. *et al.* Inferring the deep past from molecular data. *Genome Biol. Evol.* (2021) doi:10.1093/gbe/evab067.

62. Vosseberg, J. *et al.* Timing the origin of eukaryotic cellular complexity with ancient duplications. *Nat Ecol Evol* **5**, 92–100 (2021).

63. Hua, Z.-S. *et al.* Genomic inference of the metabolism and evolution of the archaeal phylum Aigarchaeota. *Nat. Commun.* **9**, 2832 (2018).

64. Chen, L.-X. *et al.* Candidate Phyla Radiation Roizmanbacteria From Hot Springs Have Novel and Unexpectedly Abundant CRISPR-Cas Systems. *Front. Microbiol.* **10**, 928 (2019).

65. Langmead, B. & Salzberg, S. L. Fast gapped-read alignment with Bowtie 2. *Nat. Methods* **9**, 357–359 (2012).

66. Kang, D. D., Froula, J., Egan, R. & Wang, Z. MetaBAT, an efficient tool for accurately reconstructing single genomes from complex microbial communities. *PeerJ* **3**, e1165 (2015).

67. Dick, G. J. *et al.* Community-wide analysis of microbial genome sequence signatures. *Genome Biol.* **10**, R85 (2009).

68. Brown, C. T. *et al.* Unusual biology across a group comprising more than 15% of domain Bacteria. *Nature* **523**, 208–211 (2015).

69. Flores, G. E. *et al.* Inter-field variability in the microbial communities of hydrothermal vent deposits from a back-arc basin. *Geobiology* **10**, 333–346 (2012).

70. Bolger, A. M., Lohse, M. & Usadel, B. Trimmomatic: a flexible trimmer for Illumina sequence data. *Bioinformatics* **30**, 2114–2120 (2014).

71. Crusoe, M. R. *et al.* The khmer software package: enabling efficient nucleotide sequence analysis. *F1000Res.* **4**, 900 (2015).

72. Li, D., Liu, C.-M., Luo, R., Sadakane, K. & Lam, T.-W. MEGAHIT: an ultra-fast single-node solution for large and complex metagenomics assembly via succinct de Bruijn graph. *Bioinformatics* vol. 31 1674–1676 Preprint at https://doi.org/10.1093/bioinformatics/btv033 (2015).

73. Li, D. *et al.* MEGAHIT v1.0: A fast and scalable metagenome assembler driven by advanced methodologies and community practices. *Methods* **102**, 3–11 (2016).

74. Langmead, B., Trapnell, C., Pop, M. & Salzberg, S. L. Ultrafast and memory-efficient alignment of short DNA sequences to the human genome. *Genome Biol.* **10**, R25 (2009).

75. Li, H. *et al.* The Sequence Alignment/Map format and SAMtools. *Bioinformatics* **25**, 2078–2079

(2009).

76. Parks, D. H., Imelfort, M., Skennerton, C. T., Hugenholtz, P. & Tyson, G. W. CheckM: assessing the quality of microbial genomes recovered from isolates, single cells, and metagenomes. *Genome Res.* **25**, 1043–1055 (2015).

77. Seitz, K. W., Lazar, C. S., Hinrichs, K.-U., Teske, A. P. & Baker, B. J. Genomic reconstruction of a novel, deeply branched sediment archaeal phylum with pathways for acetogenesis and sulfur reduction. *ISME J.* **10**, 1696–1705 (2016).

78. Alneberg, J. *et al.* Binning metagenomic contigs by coverage and composition. *Nat. Methods* **11**, 1144–1146 (2014).

79. Ounit, R., Wanamaker, S., Close, T. J. & Lonardi, S. CLARK: fast and accurate classification of metagenomic and genomic sequences using discriminative k-mers. *BMC Genomics* **16**, 236 (2015).

80. Bankevich, A. *et al.* SPAdes: a new genome assembly algorithm and its applications to single-cell sequencing. *J. Comput. Biol.* **19**, 455–477 (2012).

81. Peng, Y., Leung, H. C. M., Yiu, S. M. & Chin, F. Y. L. IDBA-UD: a de novo assembler for single-cell and metagenomic sequencing data with highly uneven depth. *Bioinformatics* vol. 28 1420–1428 Preprint at https://doi.org/10.1093/bioinformatics/bts174 (2012).

82. Hugoson, E., Lam, W. T. & Guy, L. miComplete: weighted quality evaluation of assembled microbial genomes. *Bioinformatics* (2019) doi:10.1093/bioinformatics/btz664.

83. Karst, S. M., Kirkegaard, R. H. & Albertsen, M. mmgenome: a toolbox for reproducible genome extraction from metagenomes. Preprint at https://doi.org/10.1101/059121.

84. Albertsen, M. *et al.* Genome sequences of rare, uncultured bacteria obtained by differential coverage binning of multiple metagenomes. *Nat. Biotechnol.* **31**, 533–538 (2013).

85. Dombrowski, N., Teske, A. P. & Baker, B. J. Expansive microbial metabolic versatility and biodiversity in dynamic Guaymas Basin hydrothermal sediments. *Nat. Commun.* **9**, 4999 (2018).

86. Huang, J.-M., Baker, B. J., Li, J.-T. & Wang, Y. New Microbial Lineages Capable of Carbon Fixation and Nutrient Cycling in Deep-Sea Sediments of the Northern South China Sea. *Appl.*

Environ. Microbiol. **85**, (2019).

87. Tréhu, A. M. *et al.* Feeding methane vents and gas hydrate deposits at south Hydrate Ridge. *Geophysical Research Letters* vol. 31 Preprint at https://doi.org/10.1029/2004gl021286 (2004).
88. Nunoura, T., Inagaki, F., Delwiche, M. E., Colwell, F. S. & Takai, K. Subseafloor microbial communities in methane hydrate-bearing sediment at two distinct locations (ODP Leg204) in the cascadia margin. *Microbes Environ.* **23**, 317–325 (2008).
89. Inagaki, F. *et al.* Biogeographical distribution and diversity of microbes in methane hydrate-bearing deep marine sediments on the Pacific Ocean Margin. *Proc. Natl. Acad. Sci. U. S. A.* **103**, 2815–2820 (2006).
90. Martin, M. Cutadapt removes adapter sequences from high-throughput sequencing reads. *EMBnet.journal* vol. 17 10 Preprint at https://doi.org/10.14806/ej.17.1.200 (2011).
91. Dombrowski, N., Seitz, K. W., Teske, A. P. & Baker, B. J. Genomic insights into potential interdependencies in microbial hydrocarbon and nutrient cycling in hydrothermal sediments. *Microbiome* **5**, 106 (2017).
92. Parks, D. H. *et al.* Author Correction: A complete domain-to-species taxonomy for Bacteria and Archaea. *Nat. Biotechnol.* **38**, 1098 (2020).
93. Romalde, J. L., Balboa, S. & Ventosa, A. *Microbial Taxonomy, Phylogeny and Biodiversity*. (Frontiers Media SA, 2019).
94. Wang, H.-C., Minh, B. Q., Susko, E. & Roger, A. J. Modeling Site Heterogeneity with Posterior Mean Site Frequency Profiles Accelerates Accurate Phylogenomic Estimation. *Syst. Biol.* **67**, 216–235 (2018).
95. Lagkouvardos, I. *et al.* IMNGS: A comprehensive open resource of processed 16S rRNA microbial profiles for ecology and diversity studies. *Sci. Rep.* **6**, 33721 (2016).
96. Wickham, H. *et al.* Welcome to the Tidyverse. *Journal of Open Source Software* vol. 4 1686 Preprint at https://doi.org/10.21105/joss.01686 (2019).
97. Seemann, T. Prokka: Rapid prokaryotic genome annotation. *Bioinformatics* **30**, 2068–2069 (2014).

628 98. Chan, P. P. & Lowe, T. M. tRNAscan-SE: Searching for tRNA Genes in Genomic Sequences. in
629 *Gene Prediction: Methods and Protocols* (ed. Kollmar, M.) 1–14 (Springer New York, 2019).
630 99. Buchfink, B., Xie, C. & Huson, D. H. Fast and sensitive protein alignment using DIAMOND. *Nat.*
631 *Methods* **12**, 59–60 (2015).
632 100. Miele, V., Penel, S. & Duret, L. Ultra-fast sequence clustering from similarity networks with SiLiX.
633 *BMC Bioinformatics* **12**, 116 (2011).
634 101. Miele, V. *et al.* High-quality sequence clustering guided by network topology and multiple
635 alignment likelihood. *Bioinformatics* **28**, 1078–1085 (2012).
636 102. Katoh, K. & Toh, H. Recent developments in the MAFFT multiple sequence alignment program.
637 *Brief. Bioinform.* **9**, 286–298 (2008).
638 103. Remmert, M., Biegert, A., Hauser, A. & Söding, J. HHblits: lightning-fast iterative protein sequence
639 searching by HMM-HMM alignment. *Nat. Methods* **9**, 173–175 (2011).
640 104. Huerta-Cepas, J. *et al.* eggNOG 4.5: a hierarchical orthology framework with improved functional
641 annotations for eukaryotic, prokaryotic and viral sequences. *Nucleic Acids Res.* **44**, D286–93 (2016).
642 105. Makarova, K. S., Wolf, Y. I. & Koonin, E. V. Archaeal Clusters of Orthologous Genes (arCOGs):
643 An Update and Application for Analysis of Shared Features between Thermococcales,
644 Methanococcales, and Methanobacteriales. *Life* **5**, 818–840 (2015).
645 106. Finn, R. D. *et al.* Pfam: the protein families database. *Nucleic Acids Res.* gkt1223 (2013).
646 107. Jones, P. *et al.* InterProScan 5: genome-scale protein function classification. *Bioinformatics* **30**,
647 1236–1240 (2014).
648 108. Kanehisa, M., Sato, Y. & Morishima, K. BlastKOALA and GhostKOALA: KEGG Tools for
649 Functional Characterization of Genome and Metagenome Sequences. *J. Mol. Biol.* **428**, 726–731
650 (2016).
651 109. Søndergaard, D., Pedersen, C. N. S. & Greening, C. HydDB: A web tool for hydrogenase
652 classification and analysis. *Sci. Rep.* **6**, 34212 (2016).
653 110. Eddy, S. R. Accelerated Profile HMM Searches. *PLoS Comput. Biol.* **7**, e1002195 (2011).

654 111. Kelley, L. A., Mezulis, S., Yates, C. M., Wass, M. N. & Sternberg, M. J. E. The Phyre2 web portal
655 for protein modeling, prediction and analysis. *Nature Protocols* vol. 10 845–858 Preprint at
656 https://doi.org/10.1038/nprot.2015.053 (2015).
657 112. Petitjean, C., Deschamps, P., López-García, P., Moreira, D. & Brochier-Armanet, C. Extending the
658 conserved phylogenetic core of archaea disentangles the evolution of the third domain of life. *Mol.*
659 *Biol. Evol.* **32**, 1242–1254 (2015).
660 113. Katoh, K. & Standley, D. M. MAFFT multiple sequence alignment software version 7:
661 improvements in performance and usability. *Mol. Biol. Evol.* **30**, 772–780 (2013).
662 114. Criscuolo, A. & Gribaldo, S. BMGE (Block Mapping and Gathering with Entropy): a new software
663 for selection of phylogenetic informative regions from multiple sequence alignments. *BMC Evol.*
664 *Biol.* **10**, 210 (2010).
665 115. Price, M. N., Dehal, P. S. & Arkin, A. P. FastTree 2 - Approximately maximum-likelihood trees for
666 large alignments. *PLoS One* **5**, (2010).
667 116. Camacho, C. *et al.* BLAST : architecture and applications. *BMC Bioinformatics* vol. 10 421 Preprint
668 at https://doi.org/10.1186/1471-2105-10-421 (2009).
669 117. Huerta-Cepas, J. *et al.* Fast Genome-Wide Functional Annotation through Orthology Assignment by
670 eggNOG-Mapper. *Mol. Biol. Evol.* **34**, 2115–2122 (2017).
671 118. Suzek, B. E. *et al.* UniRef clusters: a comprehensive and scalable alternative for improving sequence
672 similarity searches. *Bioinformatics* **31**, 926–932 (2015).
673 119. Capella-Gutiérrez, S., Silla-Martínez, J. M. & Gabaldón, T. trimAl: a tool for automated alignment
674 trimming in large-scale phylogenetic analyses. *Bioinformatics* **25**, 1972–1973 (2009).
675 120. Nguyen, L.-T., Schmidt, H. A., von Haeseler, A. & Minh, B. Q. Iq-tree: A fast and effective
676 stochastic algorithm for estimating maximum-likelihood phylogenies. *Mol. Biol. Evol.* **32**, 268–274
677 (2015).
678 121. Guy, L., Roat Kultima, J. & Andersson, S. G. E. genoPlotR: comparative gene and genome
679 visualization in R. *Bioinformatics* vol. 26 2334–2335 Preprint at

https://doi.org/10.1093/bioinformatics/btq413 (2010).

122. Hoang, D. T., Chernomor, O., von Haeseler, A., Minh, B. Q. & Vinh, L. S. UFBoot2: Improving the Ultrafast Bootstrap Approximation. *Mol. Biol. Evol.* **35**, 518–522 (2018).

123. Martijn, J. *et al.* Hikarchaeia demonstrate an intermediate stage in the methanogen-to-halophile transition. *Nature Communications* vol. 11 Preprint at https://doi.org/10.1038/s41467-020-19200-2 (2020).

124. Huang, W.-C. *et al.* Comparative genomic analysis reveals metabolic flexibility of Woesearchaeota. *Nat. Commun.* **12**, 5281 (2021).

125. Martijn, J., Vosseberg, J., Guy, L., Offre, P. & Ettema, T. J. G. Phylogenetic affiliation of mitochondria with Alpha-II and Rickettsiales is an artefact. *Nature Ecology & Evolution* vol. 6 1829–1831 Preprint at https://doi.org/10.1038/s41559-022-01871-3 (2022).

126. Dharamshi, J. E. *et al.* Gene gain facilitated endosymbiotic evolution of Chlamydiae. *Nat Microbiol* **8**, 40–54 (2023).

127. Kim, E. *et al.* Implication of mouse Vps26b–Vps29–Vps35 retromer complex in sortilin trafficking. *Biochem. Biophys. Res. Commun.* **403**, 167–171 (2010).

128. Suzuki, S. W., Chuang, Y.-S., Li, M., Seaman, M. N. J. & Emr, S. D. A bipartite sorting signal ensures specificity of retromer complex in membrane protein recycling. *J. Cell Biol.* **218**, 2876–2886 (2019).

129. Balderhaar, H. J. K. & Ungermann, C. CORVET and HOPS tethering complexes - coordinators of endosome and lysosome fusion. *J. Cell Sci.* **126**, 1307–1316 (2013).

Figures

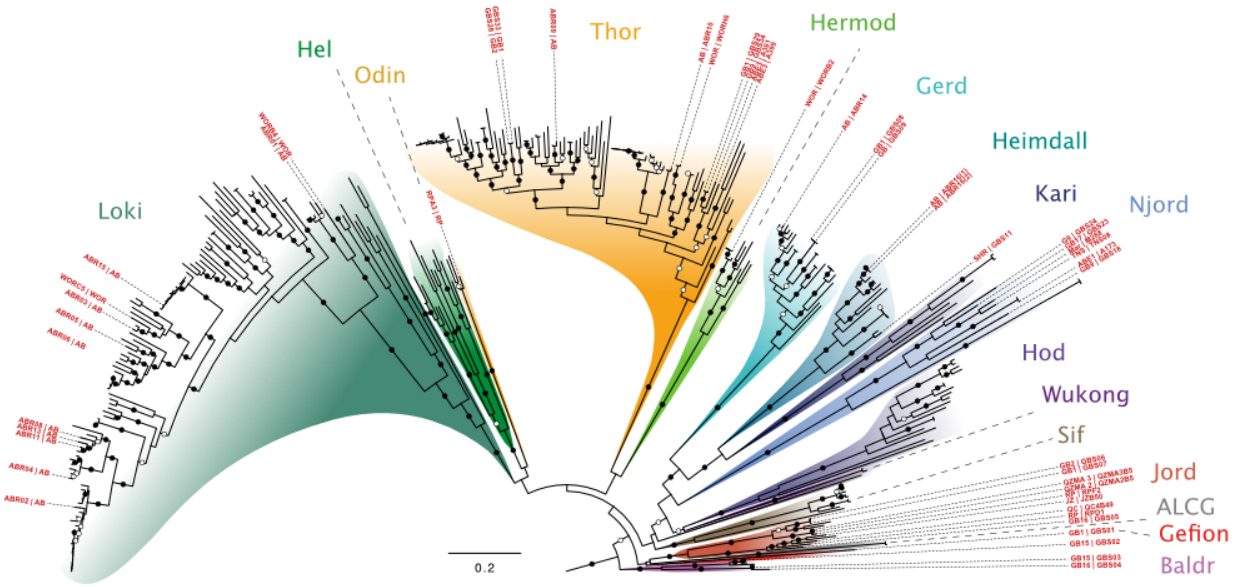

Figure 1. Phylogenomic analysis of 15 concatenated ribosomal proteins expands Asgard archaea diversity. Maximum-likelihood tree (IQ-TREE, WAG+C60+R4+F+PMSF model) of concatenated protein sequences from at least five genes, encoded on a single contig, of a 15 conserved ribosomal protein (RP15) gene cluster retrieved from publicly available and newly reported Asgard archaeal MAGs. Bootstrap support (100 pseudo-replicates) is indicated by circles at branches, with filled and open circles representing 90% and 70% support, respectively. Leaf names indicate geographical source and isolate name (inner and outer label, respectively) for the MAGs reported in this study. Scale bar denotes the average number of substitutions per site. Abbreviations: AB: Aarhus Bay (Denmark); ABE: ABE vent field, Eastern Lau Spreading Center; ALCG: Asgard Lake Cootharaba Group; CR: Colorado River (USA); GB: Guaymas Basin (Mexico); JZ: Jinze (China); LC: Loki's castle; LCB: Lower Culex Basin (USA); Mar: Mariner vent field, Eastern Lau Spreading Center; NSCS: Northern South China Sea; OWC: Old Woman Creek (USA); QC: QuCai village (China); QZM: QuZhuoMu village (China); RP: Radiata Pool

716 (New Zealand); RS: Red sea; SHR: South Hydrate Ridge; TNS: Taketomi Island (Japan); WOR:
717 White Oak River (USA).

718

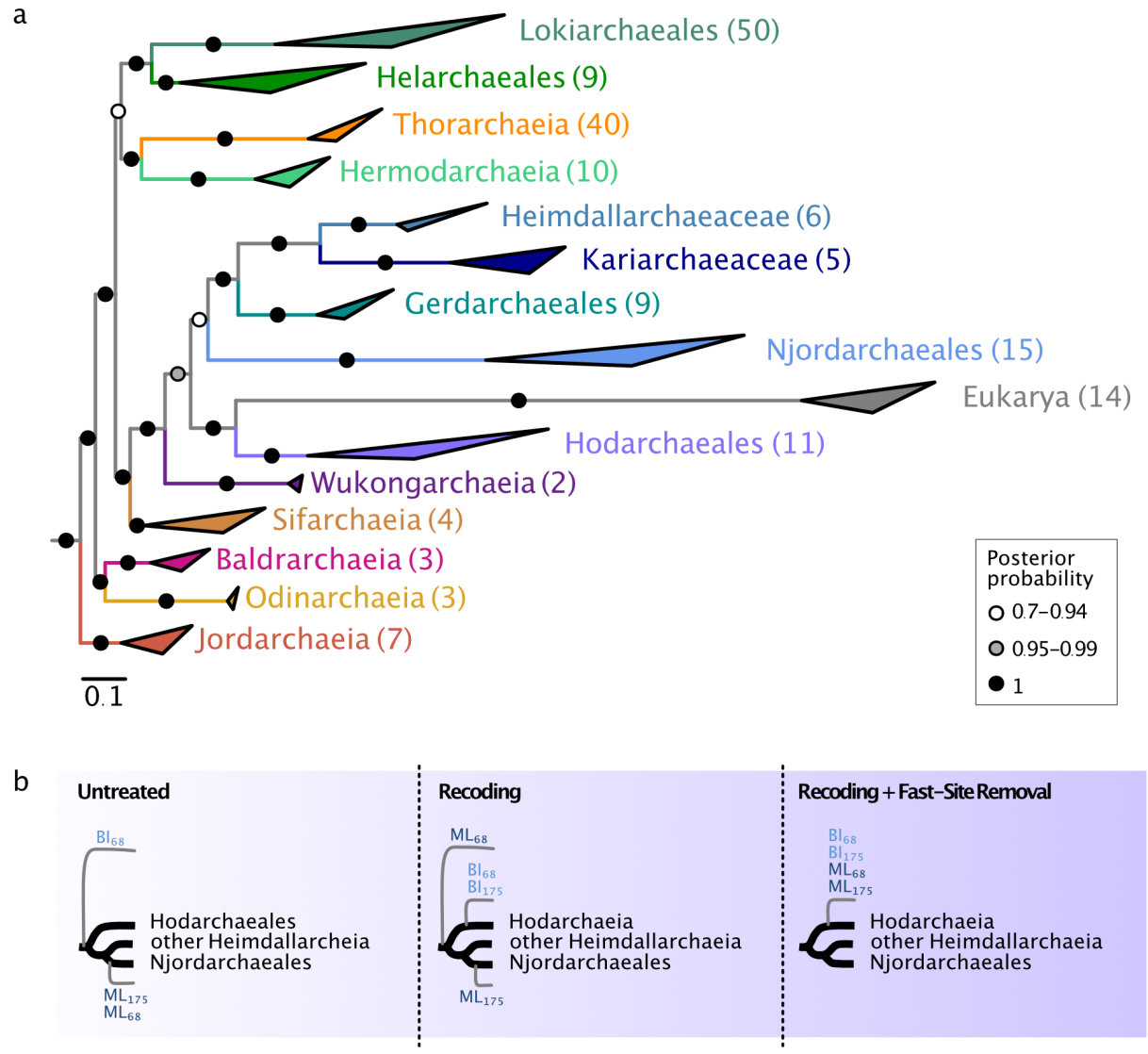

719

720 **Figure 2. Phylogenomic analyses based on 57 concatenated non-ribosomal proteins support**
721 **the emergence of eukaryotes as sister to Hodarchaeales.** a. Bayesian inference (BI) based on
722 278 archaeal taxa, using Euryarchaeota and TACK archaea as outgroup (not shown) (NM57-
723 nDK_sr4 alignment, 15,733 amino acid positions). The concatenation was SR4-recoded and

724 analyzed using the CAT+GTR model (4 chains, ~25,000 generations). b. Schematic representation
725 of the shift in the position of eukaryotes (grey branches) in ML and BI analyses of this dataset
726 under different treatments. Untreated: unprocessed dataset; Recoding: SR4-recoded dataset;
727 Recoding+Fast-Site Removal: Fast-site removal combined with SR4-recoding (the topology most
728 often recovered after removing 10% to 50% fastest-evolving sites, in steps of 10%, is shown). 175
729 and 68 refer to phylogenomic datasets containing 175 and 68 Asgard archaea, respectively. Note
730 that BI was not performed for the 175 untreated dataset due to computational limitations (for
731 detailed overview of phylogenomic analyses, see Supplementary Table 3). Scale bar denotes the
732 average expected number of substitutions per site.

733

734

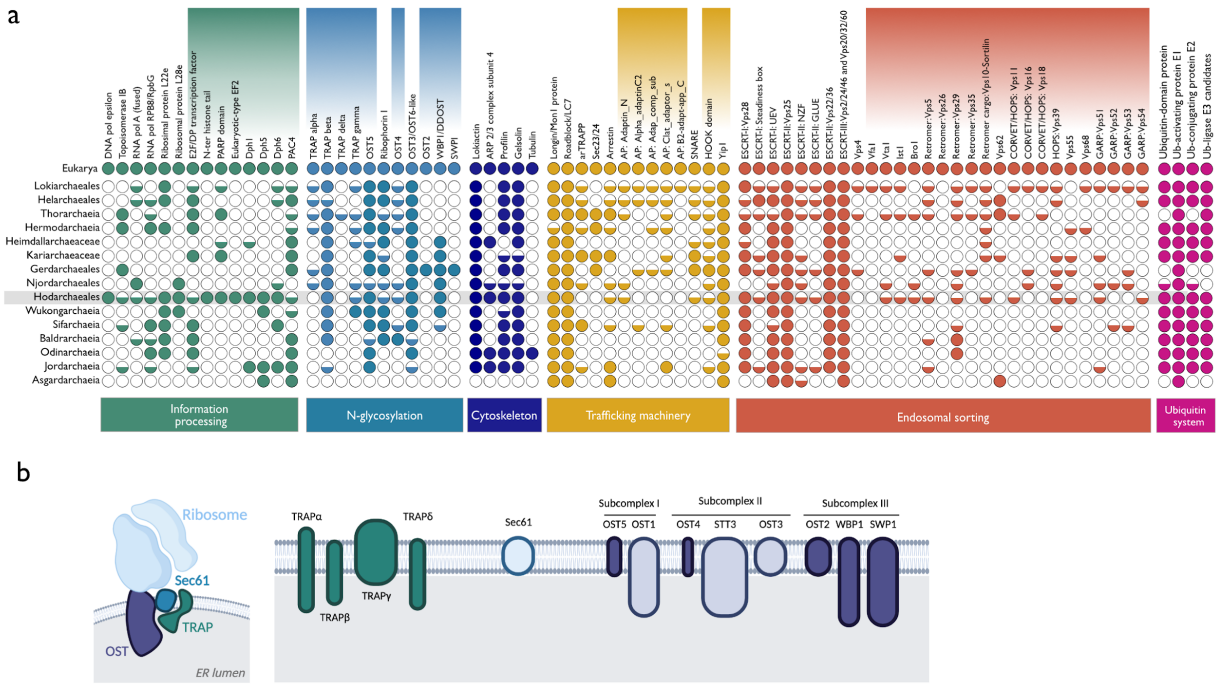

735

736 **Figure 3. Eukaryotic signature proteins in Asgard archaea.** a. Distribution of ESP homologs
737 in Asgard archaea grouped by function. Shaded rectangles above protein names indicate ESPs
738 newly identified as part of this study. Predicted homologs are depicted by colored circles: fully
739 filled circles indicate that we detected homologs in at least half of the representative genomes of
740 the clade; half-filled circles indicate that we detected homologs in fewer than half of the
741 representative genomes of the clade. Hodarchaeales homologs are highlighted with a grey
742 background. Accession numbers are available in Supplementary Table 3. b. Asgard archaea encode
743 homologs of eukaryotic protein complexes involved in N-glycosylation. The Sec61, the OST and
744 TRAP complexes are depicted according to their eukaryotic composition and localization. On the
745 right-hand side of the panel, dark-colored subunits represent eukaryotic proteins which have
746 prokaryotic homologs in Asgard archaea newly identified as part of this work; Light-colored
747 subunit homologs have been described previously[10]. Figure generated with Biorender.com.

748

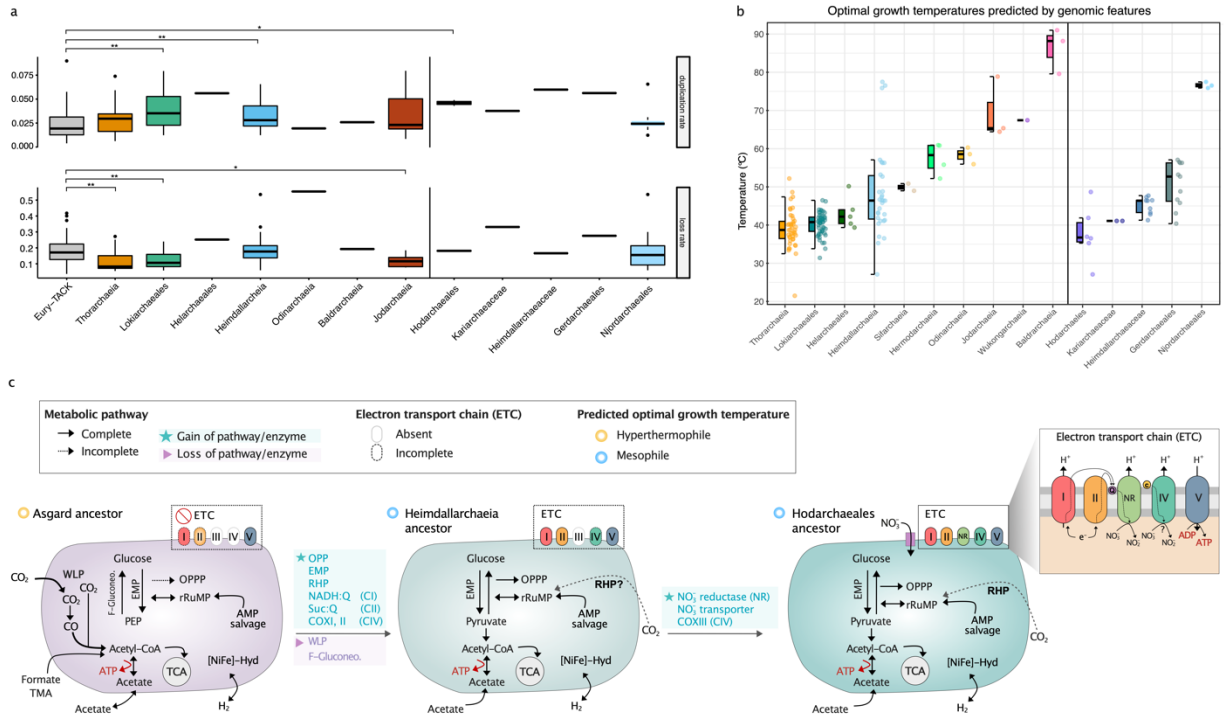

Figure 4. Genome dynamics, Optimal Growth Temperature predictions, and metabolic reconstruction of Asgard ancestors. a. Duplication (upper panel) and loss rates (lower panel) inferred for Asgard archaeal ancestors, normalized by proteome size and plotted by phylum. P-values for each Wilcoxon test against the median values of internal nodes belonging to TACK and Euryarchaeota are shown above each category, where *: p-value <= 0.05, **: p-value <=0.01, ***: p-value <=0.001. b. Optimal Growth Temperature (OGT) predictions, in degrees Celsius. OGT were predicted for the genomes presented here based on genomic and proteomic features[56] (Supplementary Table 5). Since nucleotide fractions of the ribosomal RNAs are used in this method, only those genomes with predicted rRNA genes could be analyzed. The right-hand panel depicts OGT within Heimdallarchaeia. Note that Njord- and Gerdarchaeales are predicted to be thermophiles (most genomes encode a reverse gyrase). In contrast, Hodarchaeales display the

763 lowest OGT among Heimdallarchaeia. c. Based on the presence/absence of the thermophily-
764 diagnostic enzyme reverse gyrase and the following metabolic signatures in each of the ancestors,
765 we predict that the last Asgard common ancestor probably transitioned from a hyperthermophilic
766 fermentative lifestyle to a mesophilic mixotroph lifestyle. The LAsCA likely encoded
767 gluconeogenic pathways *via* the reverse EMP gluconeogenic pathway and *via* FBP
768 aldolase/phosphatase (FBP A/P). The major energy-conserving step in the early Asgard ancestors
769 could have been the ATP synthesis by fermentation of small organic molecules (i.e., acetate,
770 formate, formaldehyde). The reverse ribulose monophosphate pathway (rRuMP) was a key
771 pathway in the LAsCA for the generation of reducing power. The Wood-Ljungdahl pathway
772 (WLP) appeared only to be present in the LAsCA and was lost in the more recent ancestors (of
773 Heimdallarchaeia and Hodarchaeales) indicated here. The tricarboxylic acid (TCA) cycle is
774 predicted to be complete in all five investigated Asgard ancestors. The inferred presence of the
775 electron transport chain (ETC) components is shown for selected ancestors of major Asgard
776 archaea groups, with the Hodarchaeales common ancestor encoding the most complete set of ETC
777 subunits, and likely using nitrate as a terminal electron acceptor. Therefore, membrane-associated
778 ATP biosynthesis coupled to the oxidation of NADH and succinate and reduction of nitrate to
779 nitrite within the respiratory chain could have been present in the LAECA. Abbreviations: Q:
780 quinone; c: cupredoxin; FBP A/P: Fructose 1,6-bisphosphate aldolase/phosphatase; EMP:
781 Embden-Meyerhof-Parnas; OPPP: Oxidative pentose phosphate pathway; rRuMP: Reversed
782 ribulose monophosphate pathway; RHP: reductive hexulose-phosphate; RuBisCO: Ribulose-1,5-
783 bisphosphate carboxylase/oxygenase; PRK: phosphoribulokinase; AMP: adenosine
784 monophosphate salvage pathway. Details of copy numbers of key enzymes involved in central
785 carbon metabolism are found in Supplementary Table 4.

Methods

Sample collection, sequencing, assembly and binning

We sampled aquatic sediments from eleven geographically distant sites: Guaymas Basin (Mexico), Lau Basin (Eastern Lau Spreading Center and Valu Fa Ridge, south-west Pacific Ocean), Hydrate Ridge (offshore of Oregon, USA), Aarhus Bay (Denmark), Radiata Pool (New Zealand), Taketomi Island Vent (Japan), the White Oak River estuary (USA), and Tibet Plateau and Tengchong (China) (Supplementary Table 1).

a. Jordarchaeote JZB50, QC4B49, QZMA23B3, QZMA2B5, QZMA3B5

Hot spring sediment samples were collected from Tibet Plateau and Yunnan Province (China) in 2016. The microbial community compositions have been described and reported previously[63,64]. Samples were collected from the hot spring pools using a sterile iron spoon into 50 ml sterile plastic tubes, then transported to the lab on dry ice, and stored at -80ºC for DNA extraction. The genomic DNA of the sediment samples was extracted using FastDNA Spin Kit for Soil (MP Biomedicals, Irvine, CA) according to the manufacturer's instructions. The obtained genomic DNA was purified for library construction, and sequenced on an Illumina HiSeq2500 platform (2 X 150 bp). The raw reads were filtered to remove Illumina adapters, PhiX and other Illumina trace contaminants with BBTools v38.79, and low-quality bases and reads using Sickle (v1.33; https://github.com/najoshi/sickle). The filtered reads were assembled using metaSPAdes (v3.10.1) with a kmer set of "21, 33, 55, 77, 99, 127". The filtered reads were mapped to the corresponding assembled scaffolds using bowtie2 v2.3.5.1[65]. The coverage of a given scaffold was calculated using the command of "jgi_summarize_bam_contig_depths" in MetaBAT v2.12.1[66]. For each sample, scaffolds with a minimum length of 2.5 kbp were binned into genome bins using MetaBAT v2.12.1, with both tetranucleotide frequencies (TNF) and scaffold coverage information

809 considered. The clustering of scaffolds from the bins and the unbinned scaffolds was visualized
810 using ESOM with a minimum window length of 2.5 kbp and max window length of 5 kbp, as
811 previously described[67]. Misplaced scaffolds were removed from bins and unbinned scaffolds
812 whose segments were placed within the bin areas of ESOMs were added to the corresponding bins.
813 Scaffolds with a minimum length of 1 kbp were uploaded to ggKbase
814 (http://ggkbase.berkeley.edu/). The ESOM-curated bins were further evaluated based on
815 consistency of GC content, coverage and taxonomic information, and scaffolds identified with
816 abnormal information were removed. The ggKbase genome bins were curated individually to fix
817 local assembly errors using ra2.py [68].

818 *b. Njordarchaeote A173, A3132, M288 and Thorarchaeote A361, A381, A399*

819 Hydrothermal vent deposits were collected from the ABE (ABE 1, 176° 15.48'W, 21° 26.68'S,
820 2142 m; ABE 3, 176° 15.59'W, 21° 26.95'S, 2131 m) and Mariner (176° 36.07'W, 22° 10.81'S,
821 1914 m) vent fields along the Eastern Lau Spreading Center in April/May of 2015 during the
822 RR1507 Expedition on the RV Roger Revelle. Sample collection and processing were done as
823 previously described[69]. DNA was extracted from homogenized rock slurries using the DNeasy
824 PowerSoil kit (Qiagen) as per the manufacturer's instructions. Samples were prepared for
825 sequencing on the Illumina HiSeq 3000 using Nextera DNA Library Prep kits (Illumina), and
826 metagenomes (2x150 bp) were sequenced at the Oregon State University Center for Genome
827 Research and Computing. Trimmomatic[70] v.0.36 was used to trim low-quality regions and adapter
828 sequences from raw reads (parameters: ILLUMINACLIP:TruSeq3-PE-2.fa:2:30:10,
829 LEADING:20, SLIDINGWINDOW:4:20, MINLEN:50). Clean paired reads were then interleaved
830 using the khmer software package[71]. Interleaved and unpaired reads were assembled with
831 MEGAHIT v.1.1.1-2-g02102e1 (--k-min 31, --k-max 151, --k-step 20, --min-contig-len 1000)

[72,73]. Trimmed reads were mapped back to the contigs to determine read coverage using Bowtie 2 v.2.2.9 [65,74] and SAMtools v.1.3.1[75]. Binning was performed with MetaBAT v.0.32.4[66] using tetranucleotide frequency and read coverage. Bin completion and contamination were estimated with CheckM v.1.0.7[76].

c. *Lokiarchaeote ABR01, ABR02, ABR03, ABR04, ABR05, ABR06, ABR08, ABR11, ABR13, ABR15, Thorarchaeote ABR09, ABR10 and Heimdallarchaeote ABR14, ABR16* MAGs were obtained as previously described[31].

d. *Archaeon WORA1, WORB2, Heimdallarchaeote WORE3, Lokiarchaeote WORB4, WORC5 and Thorarchaeote WORH6*

Sampling, DNA extraction, sequencing library preparation and sequencing methods were previously described[77]. Published assemblies and raw reads for the samples WOR-1-36_30 (SAMN06268458; Gp0056175), WOR-1-52-54 (SAMN06268416; Gp0059784), WOR-3-24_28 (SAMN06268417; Gp0059785) were downloaded from JGI. Short reads were trimmed using Trimmomatic[70] v0.33 (PE ILLUMINACLIP:2:30:10 SLIDINGWINDOW:4:15 MILEN:100). Contigs shorter than 1000 bp were excluded from the assembly using SeqTK v1.0r75 (https://github.com/lh3/seqtk). Each assembly was binned using CONCOCT v0.4.1[78] and coverage information from the three datasets, and Asgard bins were subsequently identified based on phylogenies of concatenated ribosomal proteins[10]. Identified Asgard MAGs were used together with publicly available Asgard genomes to recruit trimmed-reads originated from Asgard genomes using CLARK v1.2.3 with the -m 0 option[79]. For each dataset, recruited Asgard reads were independently assembled using SPAdes[80] and IDBA-UD[81] and further binned using CONCOCT, using a minimum contig length of 1000 bp. Bins with higher completeness and lower contamination values as predicted by miComplete v1.00[82] were selected and manually curated

using mmgenome v0.7.1[83,84] using the coverage information, paired-reads linkage, composition and marker genes information. The samples and assembly method used for each final MAG were: Archaeon WORA1 (WOR-1-52-54; spades), Archaeon WORB2 (WOR-1-52-54; IDBA-UD), Heimdallarchaeote WORE3 (WOR-3-24_28; spades), Lokiarchaeote WORB4 and WORC5 (WOR-1-36_30; IDBA-UD), and Thorarchaeote WORH6 (WOR-1-36_30; spades).

e. Jordarchaeote RPD1, RPF2 and Odinarchaeote RPA3

Information about the location of the hot spring sediments from Radiata Pool, sampling and DNA extraction procedures was previously reported[10]. Short paired-end Illumina reads were generated and preprocessed using Scythe (https://github.com/vsbuffalo/scythe) and Sickle (https://github.com/najoshi/sickle) to remove adapters and low-quality reads. Reads were subsequently assembled of IDBA-UD 1.1.3 (--maxk 124). The Jordarchaeote RPF2 MAG was generated by binning contigs according to their tetranucleotide frequencies using esomWrapper.pl (https://github.com/tetramerFreqs/Binning) with a minimum contig length 5000 bp and a window size of 10 Kbp. ESOM maps were manually delineated using the Databionic ESOM viewer (http://databionic-esom.sourceforge.net/). Jordarchaeote RPD1 and Odinarchaeote RPA3 were binned following the methodology described in above (section d), but re-assembling the recruited reads only with IDBA-UD (--maxk 124)[81].

f. Jordarchaeote GBS01, GBS02, GBS03, GBS04, GBS05, GBS06, GBS07, Heimdallarchaeote GBS08, GBS09, GBS10, GBS11, Lokiarchaeote GBS14, Njordarchaeote GBS15, GBS16, GBS17, GBS18, GBS19, GBS20, GBS21, GBS22, GBS23, GBS24, GBS25, GBS26, TNS08 and Thorarchaeote GBS28, GBS29, GBS33, GBS34 MAGs were obtained as described in [85].

g. Heimdallarchaeote B3_JM_08 MAG was obtained as described in [86].

878 *h. Thorarchaeote OWC_bin2, OWC_bin3 and OWC_bin4* MAGs were obtained as described
879 in [31].

880 *i. Heimdallarchaeote GBS11*

881 Samples were made available by the Gulf Coast Repository (GCR) and were collected on the
882 Ocean drilling Program (ODP) Leg 204 at site 1244 (44°35.17N, 125°7.19W) on July 14th, 2002
883 (hole C and core 2). The ODP site is found at a water depth of 890 m on the eastern side of the
884 South Hydrate Ridge on the Cascadia Margin. This site has been well characterized physically and
885 geochemically[87]. Furthermore, the microbial community structure has been surveyed using 16S
886 rRNA gene sequencing[88,89]. Two sediment samples, designated DCO-2-5 (sample ID 1489929)
887 and DCO-2-7 (sample ID 1489924), were collected at a sediment depth of 12.40 and 14.96 m
888 below the seafloor, respectively, and stored at -80°C at GCR. A total amount of 10 g of each of
889 the two sediment samples was used to extract DNA using the MoBio DNA PowerSoil Total kit. A
890 total amount of 100 ng DNA was used to prepare sequencing libraries that were 150 bp paired-end
891 sequenced at the Marine Biological Laboratory (Woods Hole, MA, USA) on an Illumina MiSeq
892 sequencer. Adaptors and DNA spike-ins were removed from the forward and reverse reads using
893 cutadapt v1.12[90]. Afterwards, reads were interleaved using interleave_fasta.py
894 (https://github.com/jorvis/biocode/blob/master/fasta/interleave_fasta.py), and further trimmed
895 using Sickle with default settings (Fass JN) (https://github.com/najoshi/sickle). Metagenomic
896 reads from both samples were co-assembled using IDBA-UD using the following parameters:
897 --pre_correction, -mink 75, -maxk 105, --step 10, --seed_kmer 55 [81]. Metagenomic binning was
898 performed on scaffolds with a length >3,000 bp using ESOM, including a total of 4,939 scaffolds
899 with a length of 30,693,002 bp[67,81]. CheckM v1.0.5 was employed to evaluate the accuracy of the
900 binning approach by determining the percentage of completeness and contamination[76].

j. Heimdallarchaeote GBS09

MAG was obtained as previously described[91].

Exploration of phylogenetic diversity in Asgard assemblies and MAGs

To assess the presence of potential Asgard-related lineages in our assemblies, we reconstructed a phylogeny of ribosomal proteins encoded in a conserved 15-ribosomal protein (RP15) gene cluster[16]. As ingroup, we used all MAGs presented in this study, plus all genomes classified as Asgard archaea in NCBI as of June 25th 2021, plus those classified as "archaeon" corresponding to Hermodarchaeia (GCA_016550385.1, GCA_016550395.1, GCA_016550405.1, GCA_016550415.1, GCA_016550425.1, GCA_016550485.1, GCA_016550495.1, GCA_016550505.1). and all Asgard archaeal MAGs released by Sun et al.[21]. To obtain an adequate outgroup dataset, we downloaded all archaeal genomes from the Genome Taxonomy Database[92], data revision 89, and selected one genome sequence per species-level cluster as defined in https://data.gtdb.ecogenomic.org/releases/release89/89.0/sp_clusters_r89.tsv. We then selected a set of 216 genomes classified as Bathyarchaeia, Nitrososphaeria and Thermoprotei, and used them as outgroup. Genes were detected and individually aligned and trimmed as previously described[10]. Ribosomal protein sequences were selected if they were encoded in a contig containing at least five of the 15 ribosomal protein genes. ModelFinder[93] was run as implemented in IQ-TREE v. 2.0-rc2 to identify the best model among all combinations of the LG, WAG, JTT and Q.pfam models, as well as their corresponding mixture models by adding +C20, +C40 and +C60, and the additional mixture models LG4M, LG4X, UL2 and UL3, with rate heterogeneity (none, +R4 and +G4) and frequency parameters (none, +F). A PMSF approximation[94] of the chosen model (WAG+C60+R4+F) was then used for a final reconstruction using 100 non-

924 parametric bootstrap pseudoreplicates for branch statistical support. The obtained tree revealed a
925 broad genomic diversity of Asgard lineages (Figure 1).
926

927 **Environmental distribution of Asgard archaea**

928 16S rRNA gene sequences were predicted with Barrnap v 0.9
929 (https://github.com/tseemann/barrnap) with the option "--kingdom arc". Since none of the two
930 Helarchaeales bins contained 16S rRNA gene sequences, helarchaeal 16S rRNA gene sequences
931 identified by Seitz et al.[50] were used as representatives of this phylum. These sequences were
932 submitted to the IMNGS platform as queries for Paraller similarity searches against all available
933 NCBI sequence read archive (SRA) samples with a 95% similarity threshold and a minimum
934 alignment size of 200 bp[95]. Available metadata for detected SRA samples were then manually
935 assessed to link environmental context descriptions for individual SRA samples to broader
936 environment categories. The sequence abundance output file generated by IMNGS was then
937 analysed using R and the package tidyverse to calculate the number of SRA samples belonging to
938 each environment per phylum[96].
939

940 **Gene prediction**

941 Gene prediction was performed using Prokka[97] v1.12 (prokka --kingdom Archaea --norrna --
942 notrna). rRNA genes and tRNA genes were predicted with Barrnap
943 (https://github.com/tseemann/barrnap) and tRNAscan-SE[96,98], respectively.

Optimal growth temperature prediction

Optimal growth temperatures were predicted for the genomes presented here based on genomic and proteomic features[56] (see Supplementary Information). Since ribosomal RNAs nucleotide composition are used in this method, only genomes with predicted rRNAs were analyzed.

Identification of homologous protein families

All-versus-all similarity searches of all predicted proteins from the A64 taxon selection (64 Asgard, 76 TACK, 43 Euryarchaeota and 41 DPANN archaea; see Supplementary Table 2) were performed using diamond[99] blastp (--more-sensitive --evalue 0.0001 --max-target-seqs 0 --outfmt 6). The file generated was used to cluster protein sequences into homologous families using SiLiX[100] v.1.2.10, followed by Hifix[101] v1.0.6. The identity and overlap parameters required by Silix were set to 0.2 and 0.7, respectively, after inspecting a wide range of values (--ident [0.15,0.4] and --overlap [0.55-0.9], with increments of 0.05) and selecting the values that maximized the number of clusters containing at least 80% of the taxa.

Functional annotation of homologous protein families

Protein families, excluding singletons, were aligned using mafft-linsi[102] v7.402 and converted into HHsearch format (.hhm) profiles using HHblits[103] v3.0.3. Profile-profile searches were subsequently performed against a database containing profiles from EggNOG 4.5[104], arCOGs[105] and PFAM databases[106] that had been previously converted to the hhm format using HHblits[103] v3.0.3.

966

967 **Automatic functional annotation of individual proteins**

968 Individual proteins were annotated using the HMMscan tool of the HMMer suite against PFAM
969 v32[106], Interproscan[107] 5.25-64.0, EggNOG mapper v0.12.7 against the NOG database v4.5[104],
970 diamond aligner v0.9.9.110[99] against the *nr* database, arCOG[105], and GhostKoala annotation
971 server[108]. Putative hydrogenases were further classified using HydDB[109].

972

973 **Detailed analysis of ESPs**

974 In-depth analysis of potential ESPs involved a combination of automatic screens and manual
975 curation. We first manually searched for homologs of previously described ESPs[9,10,42] by using a
976 variety of sequence similarity approaches such as BLAST, HMMer tools, profile-profile searches
977 using HHblits, combined with phylogenetic inferences, and, in some cases, the Phyre2 structure
978 homology search engine[103,110,111]. We did not use fixed cutoffs, as the e-value between homologs
979 will vary depending on the protein investigated, hence the need for manual examination of
980 potential homologs and a combination of lines of evidence.

981 In addition, to identify potential new ESPs, we first used our profile-profile searches against
982 EggNOG and manually investigated Asgard orthologous groups which had a best hit to a
983 eukaryotic-specific EggNOG cluster. We also extracted PFAM domains whose taxonomic
984 distribution is exclusive to eukaryotes as per PFAM v32, and investigated cases where they
985 represented the best domain hit in Asgard archaea sequences identified by HMMscan. Finally, we
986 manually investigated dozens of proteins known to be involved in key eukaryotic functions based
987 on our knowledge and literature searches. In Figure 2, we are only reporting cases based on the

strict cutoff that the diagnostic HMM profile had the best score among all profiles detected for a protein. An exception was made for the ESCRT domain Vps28, Steadiness box, UEV, Vps25, NZF, GLUE and Vps22 domains which are usually found in combination with other protein domains and thus do not necessarily represent the best scoring domain in a protein even if they represent true homologs.

Phylogenetic analyses of concatenated proteins for species tree inference

Two sets of phylogenetic markers were used to infer the species tree. The first one (RP56) is based on a previously published dataset of 56 ribosomal proteins used to place the first assembled Asgard genomes[10]. The second one (NM57, for 'new markers') corresponds to 57 proteins extracted from a set of 200 markers previously identified as core archaeal proteins that can be used to robustly infer the tree of archaea[112]. These 57 markers were selected because they were found in at least a third of representatives of each of the 11 Asgard clades, as well as in 10 out of 14 eukaryotes, and were inherited from archaea in eukaryotes.

We initially assembled an RP56 dataset for a phylogenetically diverse set of 222 archaeal and 14 eukaryotic taxa. These included all 11 Asgard archaea MAGs and genomes available at the NCBI as of May 12, 2017, as well as the 53 most diverse novel MAGs from this work (out of 63). We gathered orthologs of these genes from all proteomes by using sequences from the previously published alignment[10,112] as queries for BLASTp. For each marker, the best BLAST hit from each proteome was added to the dataset. For the first iteration, each dataset was aligned using mafft-linsi[113] and ambiguously aligned positions were trimmed using BMGE (-m BLOSUM30)[114]. All 56 trimmed RP alignments were concatenated into an RP56-A64 supermatrix (236 taxa including

64 Asgard archaea, 6332 amino acid positions). Once this taxon set was gathered, we identified homologs of the NM57 gene set as described above, thus generating supermatrix NM57-A64 (236 taxa, 14,847 amino acid positions).

We carried out a large number of phylogenomic analyses on variations of these two RP56-A64 and NM57-A64 datasets with different phylogenetic algorithms. Notably, preparing these datasets must be done with great care and is therefore time-consuming, and subsequent phylogenomic analyses generally require an enormous amount of computational running time. However, the rapid expansion of available Asgard archaeal MAGs, notably by Liu and colleagues as of April 2021[15], urged us to update and re-run many of the computationally demanding analyses. As some of the work that was based on a more restrained taxon sampling is still deemed valuable, such as some of the Bayesian phylogenomic analyses and ancestral genome content reconstructions, we retained these in the present study.

An updated Asgard archaeal genomic sequence dataset was constructed by including all 230 Asgard archaeal MAGs and genomes available at the NCBI database as of May 12, 2021, as well as 63 novel MAGs described in the present work. All 56 trimmed RP alignments were concatenated into an RP56-A293 supermatrix (465 taxa including 293 Asgard archaea, 7112 amino acid positions), which was used to infer a preliminary phylogeny with FastTree v2[115] (Supplementary Figure 16). Given the high computational demands of the subsequent analyses, we then used this phylogeny to select a subsample of Asgard archaea representatives. For this, we first removed the most incomplete MAGs encoding fewer than 19 ribosomal proteins (i.e., 1/3 of the markers) in the matrix. We also used the preliminary phylogeny to sub-select among closely related taxa: among taxa that were separated by branch lengths of <0.1, we only kept one representative. This led to a selection of 331 genomes, including 175 Asgard archaea, 41 DPANN,

43 Euryarchaeota, and 72 TACK representatives (RP56-A175 dataset). Out of these 175 Asgard archaea, 41 correspond to MAGs newly reported here. Once this taxon set was gathered, we identified homologs of the NM57 gene set as described above, thus generating supermatrix NM57-A175. All datasets and their composition are summarized in Supplementary Table 2.

To test for potential phylogenetic reconstruction artefacts, our datasets were subjected to several treatments. Supermatrices were recoded into four categories, using the SR4 scheme[27]. The corresponding phylogenies were reconstructed with IQ-TREE (using a user-defined previously described model referred to as 'C60SR4', based on the implemented 'LG+C60' model and modified to analyze the recoded data[10]) and Phylobayes (under the CAT+GTR model)[10]. We also used the estimated site rate output generated by IQ-TREE (-wsr) to classify sites into 10 categories, from the fastest to the slowest evolving, and we removed them in a stepwise fashion, removing from 10% to 90% of the data. Finally, we combined both approaches by applying SR4 recoding to the alignments obtained after each fast-site removal step. All phylogenetic analyses performed are summarized in Supplementary Table 2. See Supplementary Information for details and discussion.

Analyses of individual proteins

For individual proteins of interest, we gathered homologs using various approaches, depending on the level of conservation across taxa. In order to detect putative Asgard homologs of eukaryotic proteins, we used a combination of tools including BLASTp[116] and the HMMer toolkit (http://hmmer.org/) if HMM profiles were available, and queried a local database containing our 240 archaeal representatives (including all Asgard predicted proteomes). We then investigated the Asgard candidates by 1) using them as seed for BLASTp searches against nr; 2) by 3D modelling

using Phyre2 and Swissmodel when sequence similarity was low; 3) by annotating them using Interproscan 5.25-64.0[107], EggNOG mapper v0.12.7[117], against the NOG database[117], and GhostKoala annotation server[108]; 4) by annotating the archaeal orthologous cluster they belonged to using profile-profile annotation as described above. Eukaryotic homologs were gathered from the UniRef50 database[118]. Depending on the divergence between homologs, they were aligned using mafft-linsi and trimmed using TrimAl[119] (--automated1) or BMGE[114], or, in cases where we investigated a specific functional domain, we used the hmmalign tool from the HMMer package with the --trim flag to only keep and align the region corresponding to this domain. When divergence levels allowed, phylogenetic analyses were performed using IQ-TREE with model testing including the C-series mixture models (-mset option)[120]. Statistical support was evaluated using 1000 ultrafast bootstrap replicates (for IQ-TREE)[119].

Ancestral reconstruction

For the ancestral reconstruction analyses, only a subset of 181 taxa were included (64 Asgard, 74 TACK and 43 Euryarchaeota, see Supplementary Table 2 for details). Protein families with more than three members were aligned and trimmed using mafft-linsi v7.402[113] and trimAl v1.4.rev15 with the --gappyout option[119]. Tree distributions for individual protein families were estimated using IQ-TREE v1.6.5 (-bb 1000 -bnni -m TESTNEW -mset LG -madd LG+C10,LG+C20 -seed 12345 -wbtl -keep-ident)[122]. The species phylogeny together with the gene tree distributions were subsequently used to compute 100 gene-tree species tree reconciliations using ALEobserve v0.4 and ALEml_undated[52,53], including the fraction_missing option that accounts for incomplete genomes. The genome copy number was corrected to account for the extinction probability per cluster (github.com/maxemil/ALE/commit/136b78e). The missing fraction of the genome was

calculated as 1 minus the completeness values (in fraction) as estimated by CheckM v1.0.5 for each of the 181 taxa[76]. Protein families containing only one protein (singletons) were considered as originations at the corresponding leaf. The ancestral reconstruction of 5 protein families that included more than 2000 proteins raised errors and could not be computed. The minimum threshold of the raw reconciliation frequencies for an event to be considered was set to 0.3 as commonly done[123–126] and recommended by the authors of ALE (Gergely Szölősi, personal communication).

Ancestral metabolic inferences

Metabolic reconstruction of the Asgard ancestors was based on the inference, annotation and copy number of genes in ancestral nodes. The presence of a given gene was scored if its copy number in the ancestral nodes was above 0.3. A protein family was scored as "maybe present" if the inferred copy number was between 0.1 and 0.3. The protein annotation of each of the clusters containing the ancestral nodes was manually verified for each of the enzymatic steps involved in the pathways detailed in Supplementary Table 4.

Data availability

The MAGs reported in this study have been deposited at DDBJ/EMBL/GenBank. BioProject IDs, BioSample IDs and GenBank assembly accession numbers are available in Supplementary Table 1 and will be released upon publication of the manuscript. All raw data underlying phylogenomic analyses (raw and processed alignments and corresponding phylogenetic trees) will be deposited

on Figshare (https://figshare.com/account/home#/projects/111912) upon publication of the manuscript.

Methods references

Acknowledgements

We thank Stephan Köstlbacher for intellectual input. We thank the Uppsala Multidisciplinary Center for Advanced Computational Science (UPPMAX) at Uppsala University and the Swedish National Infrastructure for Computing (SNIC) at the PDC Center for High-Performance Computing for providing computational resources. We thank the Japan Agency for Marine-Earth Science & Technology (JAMSTEC) for taking sediment samples from the Taketomi shallow submarine hydrothermal system, the crew of the RV Roger Revelle for assisting with the sampling of the ABE and Mariner vent fields along the Eastern Lau Spreading Center during the RR1507 Expedition. The Ngāti Tahu - Ngāti Whaoa Runanga Trust is acknowledged as *mana whenua* of Radiata Pool and associated samples, and we thank them for their assistance in access and sampling of the Ngatamariki geothermal features. Sampling in the Eastern Lau Spreading Center and Guaymas Basin (Gulf of California) was supported by the US-National Science Foundation (NSF-OCE-1235432 to A.-L. R. and NSF-OCE-0647633 to A.T.). A subset of Guaymas sediments were sequenced by the U.S. Department of Energy Joint Genome Institute, a DOE Office of Science User Facility under Contract No. DE-AC02-05CH11231 granted to ND. We thank the captain and crew of RV Aurora for assistance during sampling at Aarhus Bay. Sampling at Aarhus Bay was supported by the VILLUM Experiment project “FISHing for the ancestors of the eukaryotic cell” (grant number 17621 to A.S. and K.U.K.). This work was supported by grants of the European

Research Council (ERC Starting and Consolidator grants 310039 and 817834, respectively), the Swedish Research Council (VR grant 2015-04959), the Dutch Research Council (NWO-VICI grant VI.C.192.016), Marie Skłodowska-Curie ITN project SINGEK (H2020-MSCA-ITN-2015-675752) and the Wellcome Trust foundation (Collaborative award 203276/K/16/Z) awarded to T.J.G.E.. L.E. was supported by a Marie Skłodowska-Curie IEF (grant 704263), and by funding from the European Research Council (ERC Starting grant 803151). T.N. was supported by JSPS KAKENHI JP19H05684 within JP19H05679. W.-J.L. was supported by the National Natural Science Foundation of China (grant no. 91951205 and 92251302). D.T. was supported by the Swedish Research Council (International Postdoc grant 2018-06609). C.W.S. was supported by a Science for Life Laboratory postdoctoral fellowship (awarded to T.J.G.E. and C.W.S.) and funding from the Swedish research council (Vetenskaprådet Starting grant 2020-05071 to C.W.S.). J.L. was supported by the Wenner-Gren Foundation (fellowship 2016-0072). J.H.S. was supported by a Marie Skłodowska-Curie IIF grant (331291). This work was also supported by the Moore-Simons Project on the Origin of the Eukaryotic Cell, Simons Foundation 73592LPI to T.J.G.E. and B.J.B. (https://doi.org/10.46714/735925LPI) and Simons Foundation 812811 to L.E. (https://doi.org/10.46714/735923LPI), and NSF Division of Biological Science SBS Biodiversity: Discovery and Analysis program (1753661) to B.J.B.

Author contributions

T.J.G.E. conceived and supervised the study. A.S., K.U.K, W.H.L., Z.-S.H., A.L.R., W.-J.L., T.N., A.-L.R., M.B.S., and A.P.T. collected and provided environmental samples. E.F.C., F.H., J.H.S., N.D., K.W.S., B.J.B., L-X.C., J.F.B., and E.St.J. performed metagenomic sequence assemblies

and metagenomic binning analyses. L.E., D.T., E.F.C., K.W.S., C.W.S., J.L., B.J.B., and T.J.G.E. analyzed genomic data. L.E., D.T., E.F.C. and F.H. performed phylogenomic analyses. L.E., D.T., E.F.C., C.W.S., J.L. and T.J.G.E. investigated ESPs. E.F.C., L.E., and M.E.S. performed ancestral genome reconstruction analyses. V.D.A., B.J.B., C.W.S, L.E. and T.J.G.E. carried out metabolic inferences. L.E., D.T., E.F.C., C.W.S., V.D.A, B.J.B. and T.J.G.E. wrote, and all authors edited and approved, the manuscript.

These authors contributed equally: Laura Eme, Daniel Tamarit, Eva F. Caceres.

Competing interest declaration

The authors declare no competing financial interests.

Extended data figures

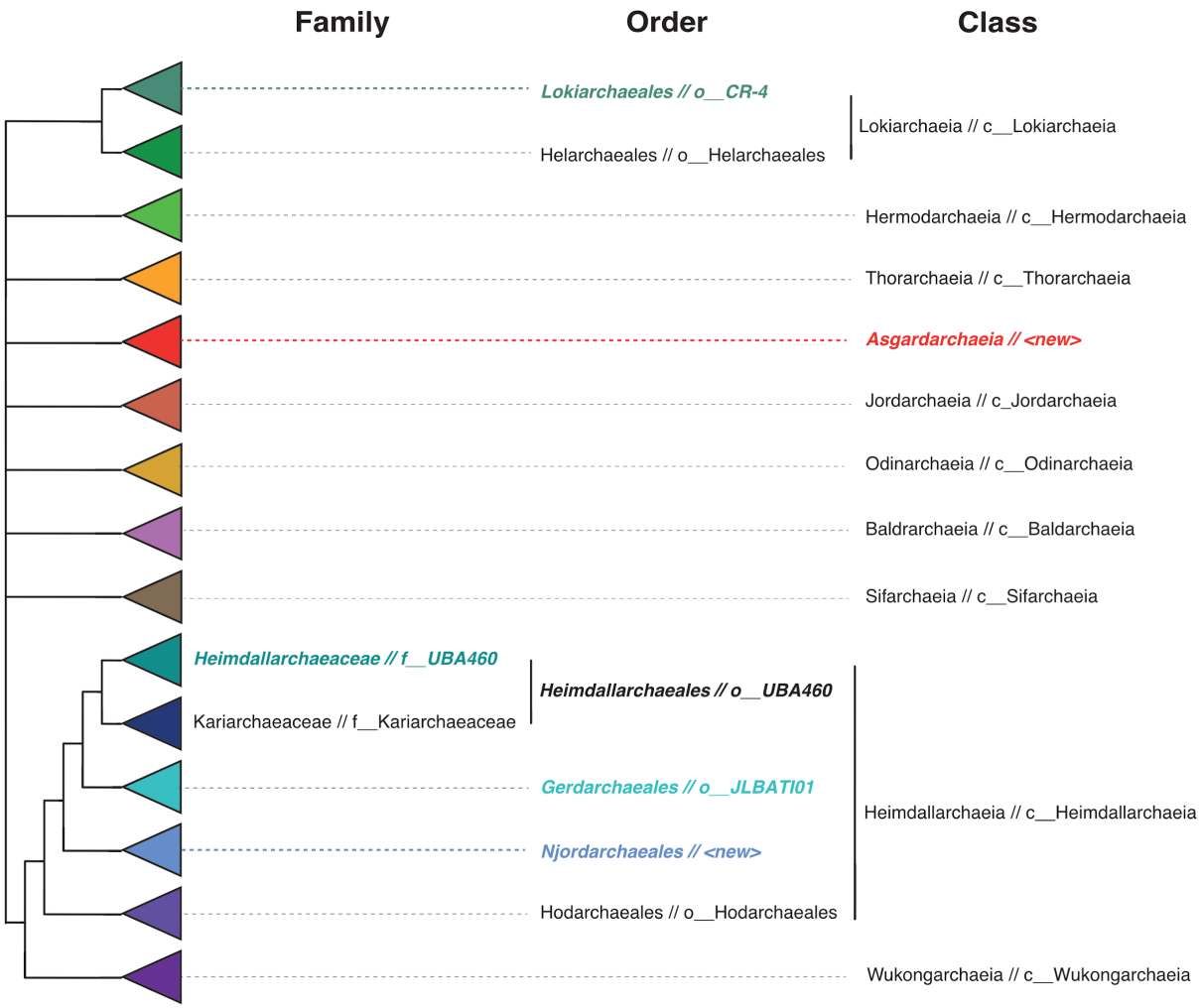

Extended Data Figure 1. Cladogram of proposed taxonomic scheme for the ranks of family, order and class for Asgard archaeal lineages employed in this study. Equivalent names in GTDB are shown after a double slash (//). Cases with differing or new names have been highlighted in colored bold italics.

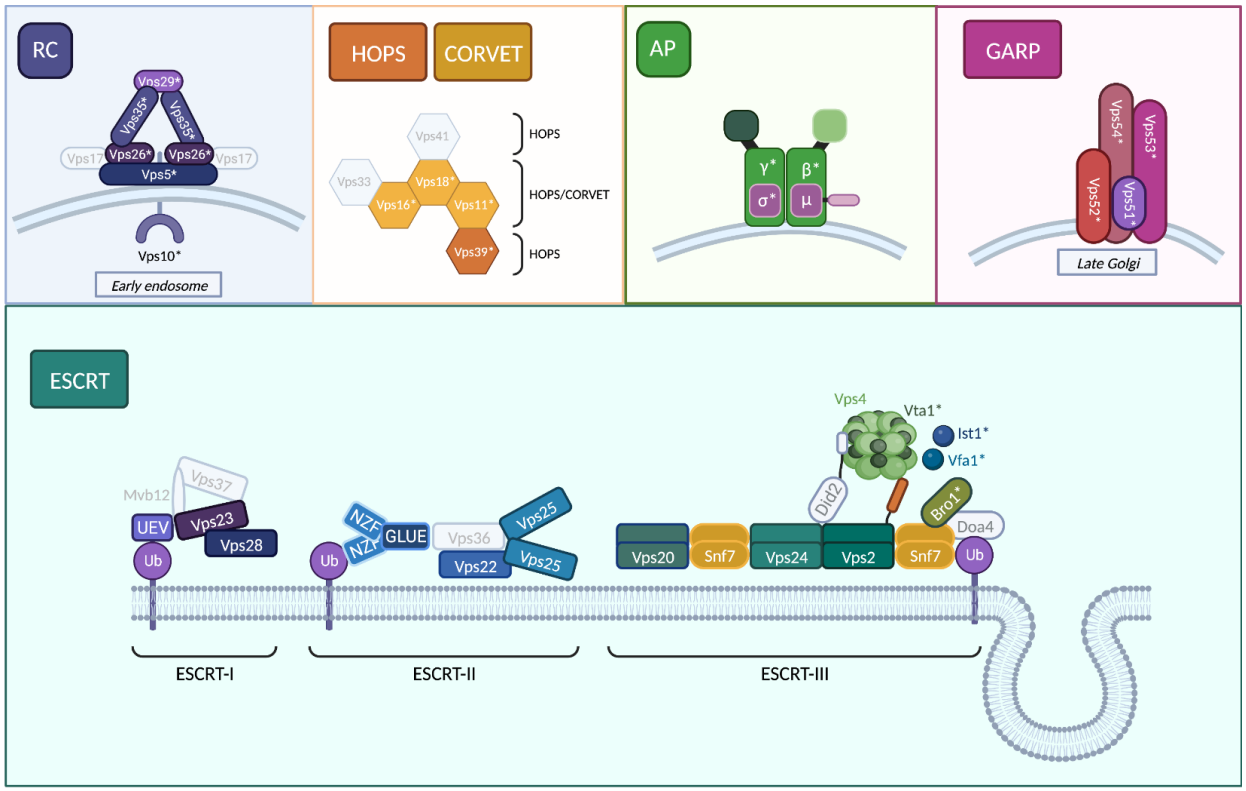

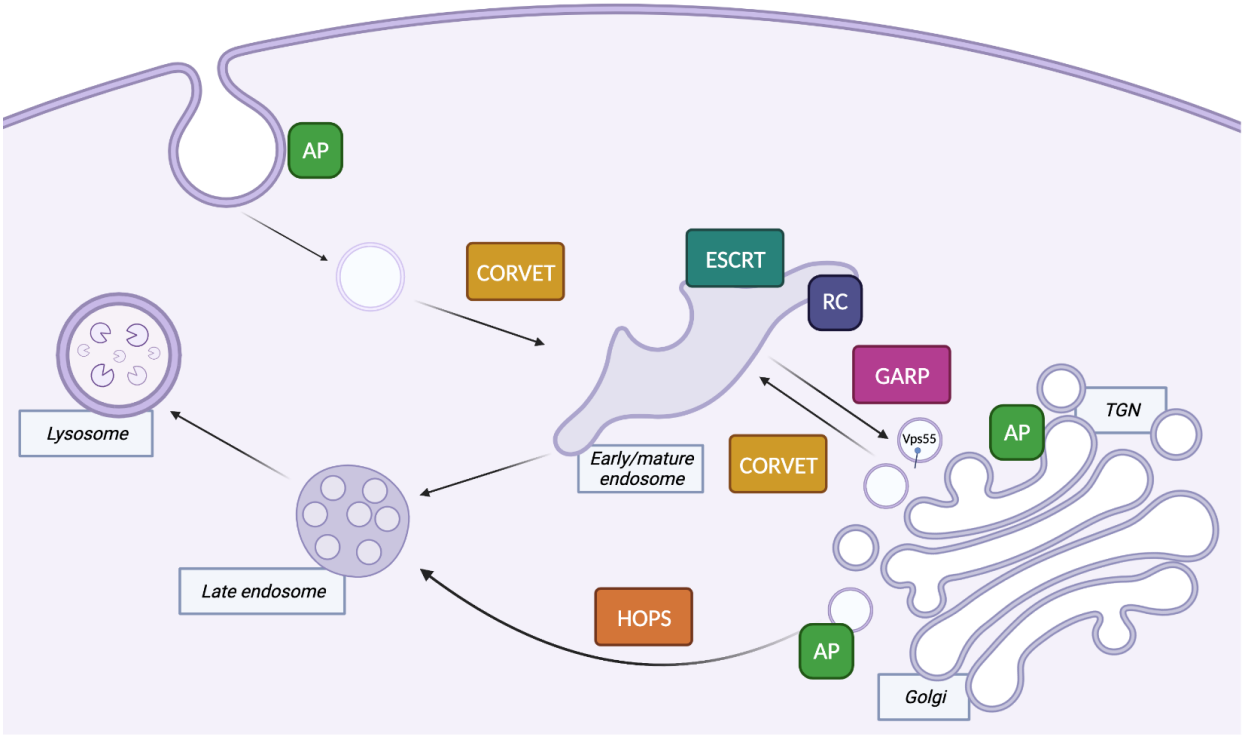

1163

1164

1165

Extended Data Figure 2. Identification of previously undetected vesicular trafficking ESPs in Asgard archaea. Schematic representation of a eukaryotic cell in which ESPs involved in membrane trafficking and endosomal sorting that have been identified in Asgard archaea are highlighted. Colored subunits have been detected in some Asgard archaea while grey ones seem to be absent from all current representatives. Only major protein complexes are depicted. Additional components can be found in Figure 2. From left to right, top to bottom: RC, Retromer complex. Retromer is a coat-like complex associated with endosome-to-Golgi retrograde traffic[36]. It is formed by Vacuolar protein sorting-associated protein 35, Vps5, Vps17, Vps26 and Vps29[127]. During cargo recycling, retromer is recruited to the endosomal membrane via the Vps5-Vps17 dimer. Cargo recognition is thought to be mediated primarily through Vps26 and possibly by Vps35. Finally, the BAR domains of Vps5-Vps17 deform the endosomal membrane to form cargo-containing recycling vesicles. Their distribution is sparse, but we have detected Asgard archaeal homologs of all subunits except for Vps17. Interestingly, the Thorarchaeota Vps5-BAR domain is often fused to Vps28, a subunit of the ESCRT machinery complex I, suggesting a functional link between BAR domain proteins and the thorarchaeial ESCRT complex. The best-characterized retromer cargo is Vps10. This transmembrane protein receptor is known in yeast and mammal cells to be involved in the sorting and transport of lipoproteins between the Golgi and the endosome. The Vps10 receptor releases its cargo to the endosome and is recycled back to the Golgi via the retromer complex[128]. CORVET: Class C core vacuole/endosome tethering complex; HOPS: Homotypic fusion and protein sorting complex. Endosomal fusion and autophagy depend on the CORVET and HOPS hexameric complexes[39]; they share the core subunits Vps11, Vps16, Vps18, and Vps33[40]. In addition, HOPS is composed of Vps41 and Vps39[41]. Vps39, found associated to late endosomes and lysosomes, promotes endosomes/lysosomes clustering and their

fusion with autophagosomes[129]. AP, Adaptor Proteins. Asgard archaea genomes from diverse phyla encode key functional domains of the AP complexes. The eukaryotic AP tetraheteromeric structure is depicted, each color corresponding to a PFAM functional domain (Medium green: Adaptin, N terminal region; Dark green: Alpha adaptin, C-terminal domain; Light green: Beta2-adaptin appendage, C-terminal sub-domain; Dark pink/clear outline: Clathrin adaptor complex small chain; Light pink/dark outline: C-ter domain of the mu subunit); all five domains were detected in Asgard archaea, although not fused to each other. GARP: Golgi-associated retrograde protein complex. The GARP complex is a multisubunit tethering complex located at the trans-Golgi network where it functions to tether retrograde transport vesicles derived from endosomes[37,38]. GARP comprises four subunits, VPS51, VPS52, VPS53, and VPS54. ESCRT: Endosomal Sorting Complex Required for Transport system. This complex machinery performs a topologically unique membrane bending and scission reaction away from the cytoplasm. While numerous components of the ESCRT-I, II and III systems have been previously detected in Asgard archaea[9,10,42], we here report Asgard homologs for several ESCRT-III regulators Vfa1, Vta1, Ist1, and Bro1. The bottom panel shows where these complexes mainly act in eukaryotic cells. Ub: Ubiquitin; Vps: vacuolar protein sorting. Subunit names in grey indicate that no homologs were detected in Asgard archaea. Domains newly identified as part of this study are indicated with an asterisk. Created with BioRender.com.

Supplementary information

Supplementary Information. This file contains Supplementary Methods, Supplementary Discussions, Supplementary Figures 1-32, Supplementary Tables 1-8, Supplementary Data and Supplementary References.

Correspondence and requests for materials should be addressed to thijs.ettema@wur.nl.